ChemComm

FEATURE ARTICLE

View Article Online
View Journal | View Issue



Cite this: *Chem. Commun.*, 2025, **61**, 2723

# Rational design and synthesis of atomically precise nanocluster-based nanocomposites: a step towards environmental catalysis

Alok Kumar, Glory James,† Ravari Kandy Aparna† and Sukhendu Mandal *

Received 6th October 2024,
Accepted 6th January 2025

DOI: 10.1039/d4cc05255b

rsc.li/chemcomm

Atomically precise metal nanoclusters (NCs) and metal–organic frameworks (MOFs) possess distinct properties that can present challenges in certain applications. However, integrating these materials to create new composite functional materials has gained significant interest due to their unique characteristics through a range of applications, particularly in catalysis. Considering MOFs as hosts and NCs as guests, several synergistic effects have been observed in composites, particularly in environmental catalytic reactions. However, the precise role of encapsulated NCs within the MOF pore structure is still in its infancy. Besides, stabilizing NCs, whether through intact ligands or without ligands *via* the MOF host, presents challenges that are currently being investigated. This feature article reviews recent advancements in the synthesis of NC@MOF composites, focusing on cutting-edge strategies for selecting MOFs and the roles of NC ligands, as well as characterization and catalytic applications.



## 1. Introduction

The swift progression of globalization and industrialization has highlighted the critical importance of sustainable environmental development.[1,2] Over the last few decades, a notable advancement has been made in creating innovative functional materials tailored for various applications.[3,4] Atomically precise metal nanoclusters (NCs), a class of nanomaterials measuring less than 2 nm, are composed of a limited number of metal atoms, ranging from a few to several hundred, and are stabilized by ligands (Scheme 1a). These nanoclusters exhibit distinct energy levels that allow them to display unique properties akin to those of molecules, including optical, magnetic, biosensing, and catalytic characteristics.[5–8] In contrast to traditional nanoparticles, the ligands attached to NCs offer significant potential for manipulating their properties to meet specific application requirements. The well-defined crystalline structures of these nanoclusters can be analyzed using X-ray crystallography, providing a crucial framework for tackling fundamental challenges and enhancing our understanding at the atomic and molecular levels, particularly in the context of environmental catalysis.[9–16]

*School of Chemistry, Indian Institute of Science Education and Research Thiruvananthapuram, Thiruvananthapuram, Kerala, 695551, India.*
*E-mail: sukhendu@iisertvm.ac.in*
† Both GJ and RKA made equal contribution.

**Alok Kumar**

*Dr. Alok Kumar received his PhD in chemistry from the Indian Institute of Technology, Kharagpur, India, in 2022. Currently, he is a National Post-doctoral Fellow (NPDF) in the group of Prof. Sukhendu Mandal at the IISERTVM. His research interest is focused on the synthesis of composite materials utilizing atomically precise nanoclusters (NCs) and metal–organic frameworks (MOFs) for enhanced value-added transformation.*

**Glory James**

*Ms. Glory James received her MSc degree in chemistry from the Indian Institute of Science Education and Research Thiruvananthapuram (IISER TVM), India. She is currently pursuing her PhD at IISER TVM. Her research centers on the synthesis, characterization, and catalytic applications of the copper metal nanocluster (MNC) incorporated metal–organic framework.*

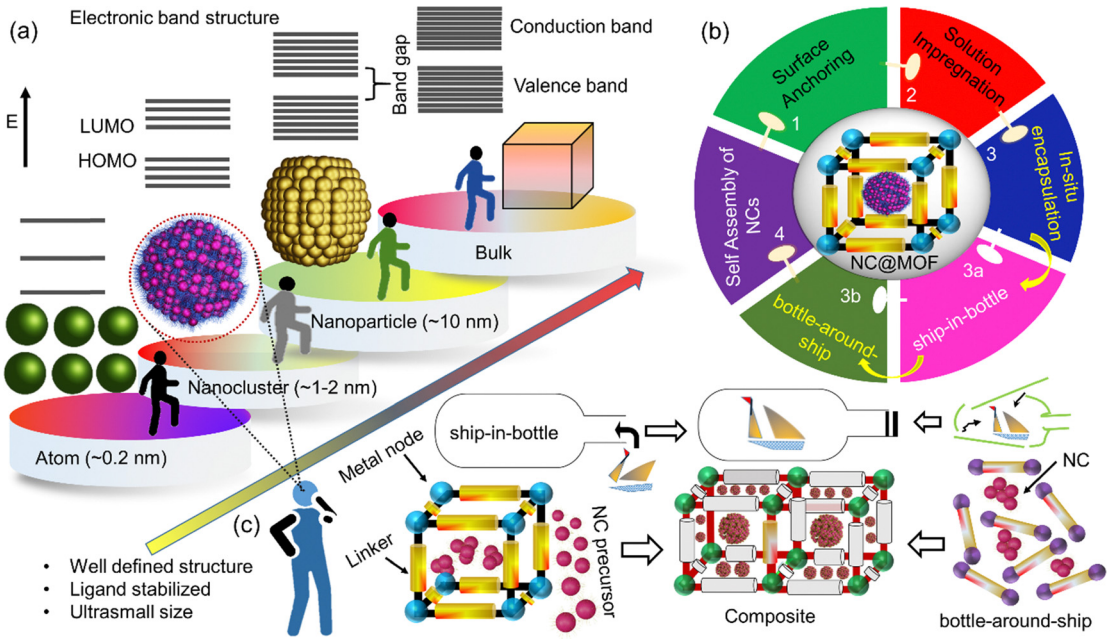


Scheme 1 (a) Schematic illustration of the size of nanoparticles and nanocluster and representation of electronic structure. (b) Flow chat presenting the strategy adopted for the synthesis of NC and MOF composite functional materials. (c) Schematic presentation of *in situ* encapsulation (ship-in-bottle and bottle-around-ship) methods.

In the realm of classical nanocatalysis, nanoparticles (NPs) such as $TiO_2$, $WO_3$, $CeO_2$, and $SiO_2$, which are primarily composed of metal oxides, are commonly utilized.[17–21] Nanoparticles (NPs) typically exhibit a polydisperse nature, and structural constraint complicates a clear correlation between the catalytic active site and the underlying mechanisms.[22,23] In recent years, NCs, have driven special attention owing to present a promising avenue for advancing fundamental value-added catalysis.[8,24] NCs as catalysts stand out due to their plentiful unsaturated active sites, high surface area, ultra-small size, atomic-level precision, and exceptional molecular purity.[6,25] However, challenges remain, particularly in addressing aggregation issues and identifying active sites hindered by steric effects from surface-bound ligands. To bridge the critical gaps in catalysis, precise ligand engineering and meticulous control over cluster atom arrangements are essential. Numerous comprehensive reviews have been documented for ligand design and synthetic methodologies for various NCs[10] including silver (Ag),[26] gold (Au),[7,27,28] silver/gold (Ag/Au) alloys,[29–31] and copper (Cu).[32] It should be emphasized that coinage metals (*e.g.*, Au, Ag), exhibit greater stability than other metal clusters (*e.g.*, Cu, Ni). This stability is attributed to the ease of synthetic process, well-established purification methods, ultra-small size (<2 nm), remarkable photo/chemical stability, and minimal toxicity. The characteristics of NCs are largely dictated by the inorganic core selected, which defines the structure of the clusters, while the ligand shell plays a crucial role in ensuring solubility and functionality within the surrounding medium.[9] Furthermore, coinage metals are known for their strong catalytic performance. However, the enhancement of properties such as efficiency, stability, selectivity, and the fine-tuning of ligand engineering remains in its early stages, prompting the exploration of diverse strategies to

**Ravari Kandy Aparna**

*Dr. Ravari Kandy Aparna received her PhD degree from the Indian Institute of Science Education and Research Thiruvananthapuram, India. Her research focuses on the synthesis, characterization, and catalytic applications of the metal nanoparticles (MNP)/metal nanocluster (MNC) incorporated Zr-based MOF composites.*

**Sukhendu Mandal**

*Dr. Sukhendu Mandal received his PhD from the Indian Institute of Science, Bangalore, India. He then pursued a postdoctoral fellowship at Pennsylvania State University, USA. Currently, he is a professor of chemistry at the Indian Institute of Science Education and Research Thiruvananthapuram, India. He works on functional molecular and nanoscale materials.*

 

improve these characteristics. Researchers have engaged in efforts to anchor NCs to various support materials, which encompass porous carbon, mesoporous silica, porous polymers, and NPs.[33–37] These support structures are generally inert concerning NC interactions or may restrict the engineering of ligands on the NCs for targeted catalytic processes. Additionally, the tendency of agglomeration on the host surface can compromise the active sites, making it crucial to select support materials that can maintain structural integrity while providing catalytic sites. Achieving a balance in both materials is desirable yet challenging. Recently, a relatively young family of porous materials known as metal–organic frameworks (MOFs) has garnered significant attention from researchers globally.[38–41] The MOFs are constructed by metal ions or clusters, which make coordinative bonds with organic linkers, resulting in three-dimensional interconnected networks. Despite their potential, MOFs face certain challenges that limit their application in catalysis. Key issues include the (a) random distribution of active sites, (b) stability concerns in various environments, and (c) low thermal and mechanical resilience due to the relatively weak bonds between metal nodes and linkers.[42,43] Nevertheless, MOFs present a unique opportunity to adjust their composition and pore structure through careful selection of precursors, synthetic methods, and post-synthetic modifications.[44] To overcome these challenges, two primary approaches have been examined: enhancing the MOF backbone through functionalization and integrating MOFs with a range of functional materials.[44–47] The composite of MOF with other functional materials, including metal NPs, quantum dots, silica, and polyoxometalates, has been thoroughly explored.[47,48] The resulting composites reveal unique chemical and physical characteristics attributed to their synergistic effects. However, it is essential to recognize the nature of the interface significantly influences the assembly process, including aspects like growth, orientation, and nucleation, which are vital for the effective development of these composites and the realization of their synergistic benefits. Among these innovative strategies, the encapsulation of NC within MOFs has sparked considerable interest in the catalytic field, leading to the development of a new class of finely tuned functional materials. Various methodologies have been employed for the synthesis of composites, specifically NC@MOF, as illustrated in Scheme 1b. The deliberate design and fabrication of advanced composite catalysts, such as NC@MOF, have demonstrated superior performance compared to their bulk counterpart.[46,49,50] However, the post-immobilization of NC and MOF has revealed a leaching phenomenon during reactions, attributed to insufficient host–guest interactions.[42,49] The selection of ligand engineering and the modification of pore structures through suitable linkers and modulators present significant challenges. These factors are critical in enhancing the stability and efficacy of the composite materials, ultimately influencing their catalytic performance. Addressing these complexities is essential for advancing the development of more effective composite catalysts in various applications. Our research group engaged in the synthesis of NP/MOF composites and exotic functional materials for catalytic applications.[51–54] Despite the advancements in this field, questions remain, particularly concerning how the ligands of NC engage with the MOF. Is there a ligand present in the MOF or NC that plays a role in the encapsulation of NC? Moreover, what is the potential stability of both the MOF pore and the NC once encapsulated, given the well-defined structure? With this aim, in this feature article, we begin with the state-of-the-art synthesis strategy for nanocluster–MOF composite material followed by the interaction of NC with the MOF through linker and pore matrices. Various factors like kinetic, choice of NC ligands, MOF linkers, and their pore matrices along with recent developments in manipulating the core structure were discussed. In addition, the composite characterization technique has been highlighted. The discussion further emphasizes the enhanced activity of NC@MOF nanocomposites and the underlying reasons for this improvement in catalysis.

## 2. Synthesis of NCs@MOF

Typically, it is understood that the pure MOF framework itself collapses during the activation process (*e.g.*, solvent removal/exchange) as shown in Fig. 1b. This phenomenon could be observed in PXRD peak broadening. These findings suggest that MOFs featuring longer, flexible linkers are more susceptible to structural collapse compared to those with shorter and rigid linkers.[55,56] Therefore, the post-incorporation of guest molecules faces the challenges of maintaining the structural integrity upon encapsulation. Besides the understanding of two components, it is essential to distinguish how the guests (NCs) interact with the framework, whether through size or energy characteristics. Numerous opportunities exist for modifying the pore matrices of MOFs, and effective fabrication strategies could be achieved through careful consideration: (a) judicial choice of a linker (Fig. 1c), (b) metal node engineering, and (c) suitable templating or defect engineering (Fig. 1a). Different strategies have been adopted over the years for the synthesis of NC/MOF composites system. These methods can generally be classified into three categories: (A) post-synthetic modification, (B) *in situ* encapsulation, and (C) self-assembly of nanocomposites. A comprehensive discussion of these techniques, along with their pros and cons, are provided in the subsequent sections.

### 2.1. Post-synthetic modification

Firstly, both components are synthesized prior to their integration. The first step involves the preparation of the MOF, which is subsequently subjected to post-synthetic modification through treatment with a pre-synthesized nanocluster. The MOF can be altered in two distinct ways: the NCs may either anchor to the surface of the MOF (termed surface anchoring) or diffuse into the MOF's pores, referred to as solution impregnation. These techniques face difficulties in establishing the composite system, primarily due to the absence of confinement and stabilization effects.

**2.1.1. Surface anchoring method.** Surface anchoring is the easiest method for combining NCs and MOFs, and it may be executed through a simple wet impregnation process. Typically,

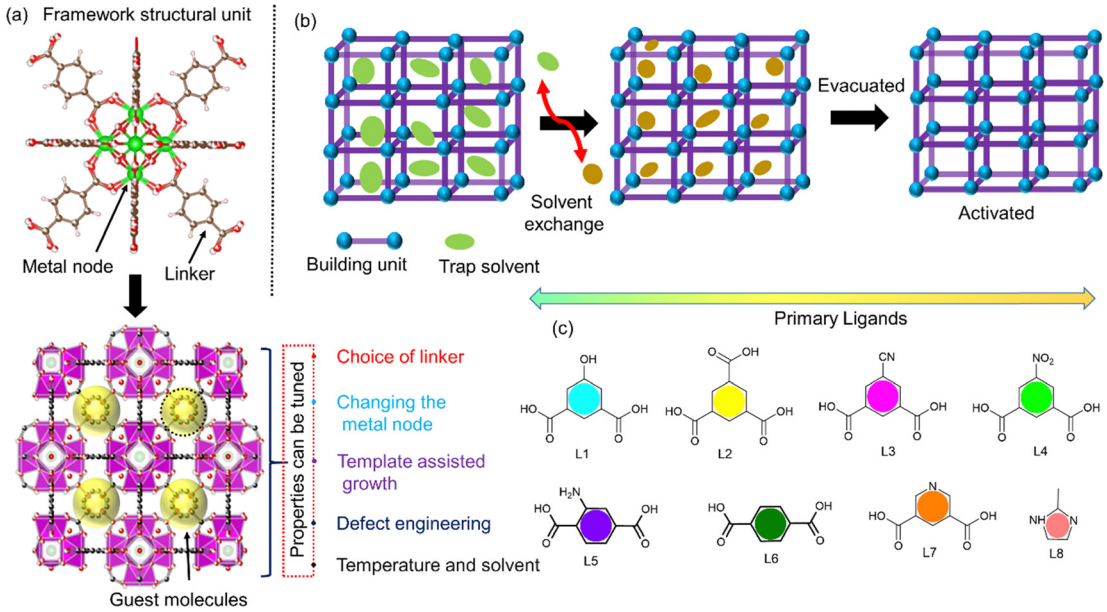


Fig. 1 (a) Depicted is UiO-66[57] with metal nodes, linker (top), and purple polyhedral (below). The void space of the pore is emphasized in a yellow sphere. (b) A repressive model for MOF activation by solvent exchange and evacuation. (c) Representative ligands for MOF framework construction, which have scope to tune the pore size, functional interactions, and rigid structure. 5-Hydroxyisophthalic acid (L1), benzene-1,3,5-tricarboxylic acid (L2), 5-cyanoisophthalic acid (L3), 5-nitroisophthalic acid (L4), 2-aminoterephthalic acid (L5), terephthalic acid (L6), pyridine-3,5-dicarboxylic acid (L7), and 2-methyl imidazole (L8).

a pre-synthesized NC is treated with a pre-synthesized MOF when the size of the MOF's apertures is smaller than that of the NC, which inhibits the cluster from penetrating the pores of the MOF. The proper anchoring through the functional group interaction by either NC ligands or MOF likers helps to inhibit the aggregation. This technique demonstrates greater effectiveness when interaction between the NC and the MOF, which may include covalent bonding, electrostatic interactions, coordination interactions, *etc.* The strength of interaction will contribute to the immobilization and stabilization of the NC with the MOF to a certain degree; however, under extreme conditions, aggregation may occur, leading to the formation of larger particles due to the lack of confinement effects offered by the MOF framework. Zhu *et al.* reported a stabilized cluster through a coordination interaction, $Au_{11}Ag_{39}$/ZIF-8, $Ag_{40}$/ZIF-8, $Au_{12}Ag_{32}$/ZIF-8, $Ag_{46}Au_{24}$/ZIF-8, $Au_4Cu_4$/ZIF-8, and $Pd_3Cl$/ZIF-8 by employing the "Exploiting Fracture Strategy" (EFS) as illustrated in Fig. 2a. A pre-synthesized ZIF-8 was modified by annealing at 300 °C, which led to the breakage of Zn–N bonds in the MOF.[58] This modification created defect sites on the MOF, which assisted in enhancing the interaction between the NC and MOF. This strategy ensured the universality of the cluster binding with the MOF as it could form a composite with all kinds of S/P-protected NC of different sizes and charges (*e.g.*, neutral, negative, and positive). Unlike the electrostatic-based strategy, only a negatively charged NC could form the composite with the MOF.[59] Zhu's group reported another composite system that utilized a covalent bridge approach to integrate NC with MOF. In this method, a pre-synthesized $Au_{25}$(L-Cys)$_{18}$ and $Au_{25}(PET)_{18}$ NC were introduced to the UiO-66-$NH_2$ MOF.[60] In the case of $Au_{25}$(L-Cys)$_{18}$, the terminal carboxylic group served as a protecting group and formed a covalent linkage with the amino group of the UiO-66-$NH_2$ MOF through a dehydration condensation reaction, leading to formation of UiO-66-$NH_2$-$Au_{25}$(L-Cys)$_{18}$. The resultant amide bond formation was confirmed using FTIR studies, which indicates the covalent bond linkage between the NC and the MOF, thereby the synergistic effect between the MOF and the NC helps in stabilizing and preventing the aggregation of the $Au_{25}$(L-Cys)$_{18}$ NC. The $Au_{25}(PET)_{18}$/UiO-66-$NH_2$ showed a significant aggregation of the NC due to a lack of interaction between the MOF and the NC, highlighting the importance of the covalent bonding in the previous case. This revealed that lack of stabilization of interaction at the interface between the MOF and the NC might cause the cluster to aggregate, ultimately forming larger-sized particles.

Luo *et al.* developed a nanocomposite ($Au_{25}$/ZIF-8), in which the coordination between the terminal carboxylic protecting group of the $Au_{25}(GSH)_{18}$ nanocluster and the $Zn^{2+}$ ions located at the nodes of MOF serves to stabilize the composite structure.[62] This anchoring of the NC on the surface of the MOF provided unrestricted access to all the reactant molecules for the reduction of 4-nitrophenol in less than 12 minutes as compared to its counterpart $Au_{25}$@ZIF-8, which took several hours for the catalytic process due to the diffusion selectivity provided by the ZIF-8 matrices. Zhu's group reported another work that uses the post-immobilization method for a nanocomposite system ZIF-8@$Au_{25}$@ZIF-67.[63] The pre-synthesized MOF (ZIF-8) and $Au_{25}$(L-Cys)$_{18}$ were used for composite formation *via* surface anchoring technique. The interaction of the terminal –COOH

 

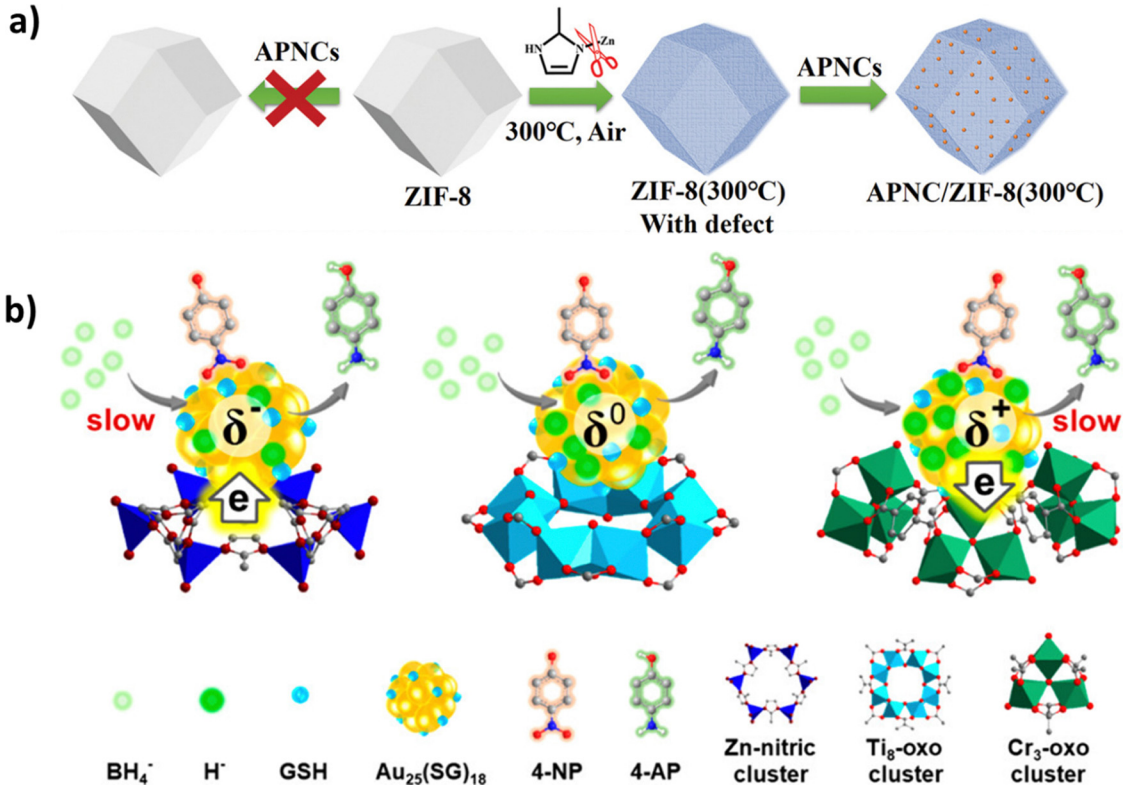


Fig. 2 (a) Schematic illustration of the synthetic route for the formation of the APNC/ZIF-8 (300 °C) composite system. Reproduced with permission from ref. 58. (b) Illustration of the charge transfer between $Au_{25}(SG)_{18}$ and metal–oxo/nitric clusters in MOFs and the reaction scheme of 4-NP reduction. Reproduced with permission from ref. 61.

group on the ZIF-8 played a crucial role in the formation of the $Au_{25}$/ZIF-8 composite. Subsequently, varying quantities of ZIF-67 precursors, specifically $Co(NO_3)_2$ and the linker 2-MeIm, were incorporated to achieve ZIF-67 coatings of differing thicknesses, resulting in the formation of the sandwich composite (ZIF-8@$Au_{25}$@ZIF-67). The authors then followed a similar procedure to synthesize the ZIF-8@$Au_{25}$@ZIF-8. To elucidate the interaction between metal nodes and NCs within a composite system, Shi *et al.* performed a theoretical study for the charge transfer dynamics involving $Au_{25}(GSH)_{18}$ NCs and the metal nodes of different MOFs, namely MIL-125 (Ti), MIL-101 (Cr), and ZIF-8 (Zn).[61] It was observed that the charge on the Au NC significantly varied depending on the interaction with the metal node. Among these three composite systems, the XPS analysis of the composite system $Au_{25}(GSH)_{18}$/MIL-125 (Ti) showed a binding energy of 84.1 eV, similar to that of unsupported $Au_{25}(GSH)_{18}$. This result confirms that the oxidation state of the Au NC is metallic $Au^0$. The $Au_{25}(GSH)_{18}$/MIL-101 (Cr) showed a positive shift in the binding energy, while $Au_{25}(GSH)_{18}$/ZIF-8 (Zn) revealed lower binding energy, unveiling Au in MIL-101 has a partial positive charge and the Au in ZIF-8 possess a partial negative charge. The reduction of 4-NP was used as a model reaction to evaluate the effect of charge on the catalytic activity of the Au NCs. $Au_{25}(GSH)_{18}$/MIL-125 and unsupported $Au_{25}(GSH)_{18}$ showed higher catalytic activity compared to the Au NCs immobilized on MIL-101 and ZIF-8. The outcome was attributed to the charge state of $Au^{\delta-}$ in the $Au_{25}(GSH)_{18}$/ZIF-8 framework, which led to the repulsion of hydride ($H^-$) species. In contrast, $Au^{\delta+}$ in the $Au_{25}(GSH)_{18}$/MIL-101 framework weakened the reductive capacity of the hydride ($H^-$) species due to a strong affinity between them (Fig. 2b). Thus, only metallic $Au^0$ demonstrated the highest activity, further highlighting the role of the MOF microenvironment in regulating the catalytic performance of encapsulated NCs.

**2.1.2. Solution impregnation method.** Initially, NC and MOF are pre-synthesized, and subsequently, the MOF is further treated with the NC to enable the encapsulation of the cluster. This technique is expected to be effective when the size of the nanocluster is smaller than the pore aperture of MOF. Due to the porous framework of the MOF, in the solution state, it will enable the diffusion of the nanocluster into the MOF matrices but this strategy has its own limitations. A key drawback of this method is the cluster's incorporation, facilitated by diffusion, carries the risk of diffusing out of the MOF. This likely to occur if the interaction between the MOF and the NC is insufficient to effectively stabilize the encapsulated structure. Thus, in solution-phase catalysis, leaching of the cluster into the solution may occur, which could lead to a decrease in catalytic efficiency. Rosi *et al.* have employed this method to synthesize bMOF-100, conducting post-synthetic ligand exchange with the MOF.[64] Authors introduced larger ligands to replace the smaller ones, which offer a descending porosity gradient in the MOF (In an outside-in fashion). The periphery had larger pore sizes as compared to the core of the MOF. A successful demonstration was observed in which a gold-thiolate nanocluster $[Au_{133}(SR)_{52}]$ was selectively incorporated at

the periphery of the bMOF-102/106 crystal through cation exchange, highlighting the size-sensitive nature of this process. This advancement paves the way for enhanced control over the molecular organization and transport in porous MOF (Fig. 3). Zhu *et al.* theoretically explored the electronic properties of Au NCs encapsulated in ZIF-8 and ZIF-90, along with their differences in CO oxidation.[65] Studies reveal that the functional groups in ZIF-8 (methyl group) and ZIF-90 (aldehyde group) lead to distinct electrical properties in the encapsulated Au NCs. Compared to Au NCs in ZIF-90, those confined in ZIF-8 exhibit stronger binding energy and greater charge transfer from the MOF framework to the Au NCs.

### 2.2. *In situ* encapsulation

In this method, the NC is integrated within the pore structure of the MOF through an *in situ* approach. There is *in situ* growth of the NC to form the resultant NC@MOF composite system. The encapsulation of the cluster utilizing this method could be achieved through two distinct approaches. The first approach involves a ''bottle around a ship'' strategy, where the MOF is constructed around pre-synthesized NC. While second approach is referred to as the ''ship in a bottle'' strategy, in which the NCs are synthesized within a pre-existing MOF (Scheme 1c).

**2.2.1. Ship-in-a-bottle method.** The process begins with the pre-synthesis of the MOF, which is subsequently immersed in a solution containing metal precursors for NC formation. These precursors diffuse into the MOF's pores and are reduced by a reducing agent to facilitate *in situ* growth of the NC. The growth of the NC is limited by the size of the MOF's pores. Additionally, an anchoring functional group (organic linker) of MOF can enhance the pore-confined growth of the NC by providing the necessary stabilization for encapsulation. This approach effectively confines the NC and minimizes its movement and aggregation into larger nanoparticles. However, achieving pure NC with atomic precision in MOF poses a significant challenge, primarily due to the lack of kinetic control over the reaction process. This method was first used by Zhu *et al.* for the successful incorporation of $Au_{11}$:$PPh_3$ in ZIF-8 MOF and $Au_{13}Ag_{12}$:$PPh_3$ in MIL-101.[66] MOFs work as a template for the growth of the cluster. The authors showed that pore-confined growth led to the formation of ultra-small NCs due to the confinement effect of the MOF, while the aggregated nanoparticles were found at the surface of the MOF. The $HAuCl_4$ was used as a precursor for the Au NC. Further, the reduction was carried out (*in situ*) using $NaBH_4$ for the formation of $Au_{11}$:$PPh_3$@ZIF-8. In addition, $AgNO_3$ along with $HAuCl_4$ was employed as a precursor for the development of $Au_{13}Ag_{12}$:$PPh_3$@MIL-101 (Fig. 4a). Fei *et al.* reported the encapsulation of the Au NC inside N-heterocyclic carbene (NHC) functionalized MOF.[67] Post-synthetic linker exchange was achieved for UiO-68-$NH_2$ to obtain the UiO-68-NHC. $HAuCl_4$ was taken as the precursor for the cluster, followed by the addition of L-glutathione (Fig. 4b). It was observed that ultrasmall NC was formed inside the pore of the MOF. The critical role of the NHC-based MOF was demonstrated by employing a similar method to incorporate the NC using amine or imidazolium-functionalized MOF. The resulting composite consists of larger gold particles, suggesting that the cluster may have aggregated due to insufficient stabilization by MOF.

Horcajada and co-workers synthesized the AgNC@MIL-125-$NH_2$ using this approach. The pre-synthesized amine-functionalized MIL-125 MOF was utilized, into which the silver precursor was integrated through an impregnation technique, subsequently followed by photoreduction to form the nanocomposite within the MOF.[68] The optimizations of irradiation time, stepwise addition of reagents, stirring conditions, and the ratio of MOF to Ag were ascertained to achieve ultrasmall. The NC was uniformly distributed within the MOF, facilitated by the amine functional group of the MOF. Szilágyi *et al.* showed how the functional group (mono- or bi-functional) of a linker in the MOF contributes to the formation of the nanocomposite. The authors synthesized the nanocomposites Pd@UiO-66-$NH_2$, Pd@UiO-66-$(NH_2)_2$, Pd@UiO-66-$CH_3$, and Pd@UiO-66-$(CH_3)_2$.[69] The findings indicated that the mono-functionalized Pd@UiO-66-$NH_2$ outperformed the bi-functionalized Pd@UiO-66-$(NH_2)_2$ in terms of encapsulating Pd NCs. This advantage is due to the strong bond formation between the Pd and the bi-functionalized MOF, which requires harsh reduction conditions for the production of Pd NCs.

In addition, the previous research indicated that an increase in the Lewis base character of a functional group enhances the encapsulation of the nanocluster, as observed with –$NH_2$ and

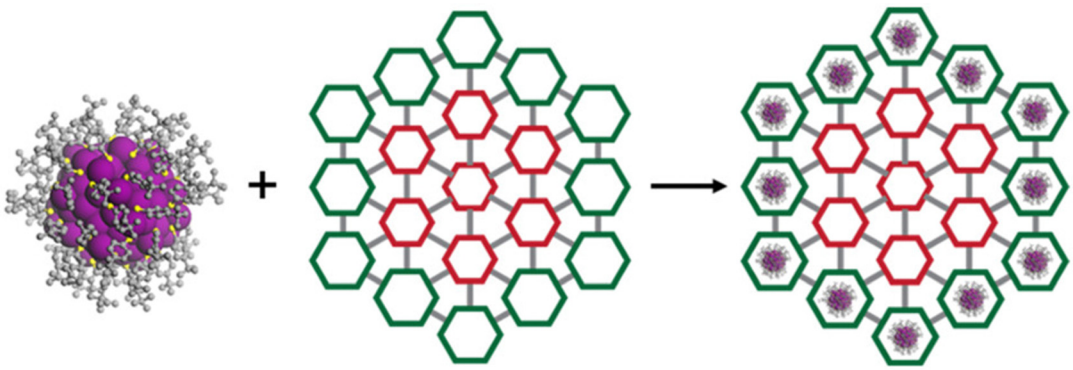

Fig. 3 Schematic representation of ''ideal'' $Au_{133}(SR)_{52}$ organization in the periphery of gradient bMOF-102/106. Reproduced with permission from ref. 64.

 

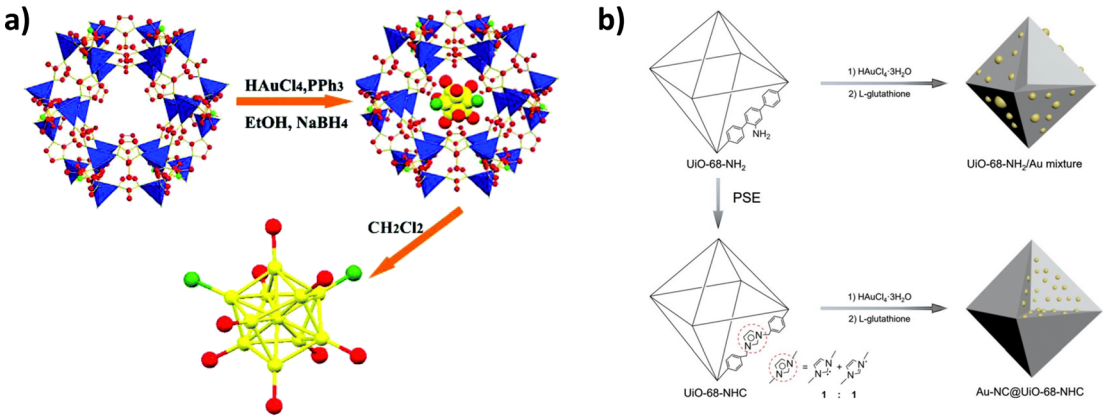


Fig. 4 (a) Schematic representation of the process of Au NCs synthesis in MOFs and the example of $Au_{11}$@ZIF-8. Reproduced with permission from ref. 66. (b) Schematic illustration of the synthesis of UiO-68-NHC, Au-NC@UiO-68-NHC, and UiO-68-$NH_2$/Au mixture. Reproduced with permission from ref. 67.

–Br groups. Conversely, a higher Lewis acidity in functional groups diminishes the likelihood of Pd encapsulation, as seen with –H, –Cl, –OH, and –$CH_3$. Notably, the Pd NC exhibited agglomeration in the presence of the $CH_3$ functionalized MOF, attributed to insufficient stabilizing interactions between the $CH_3$ group and the Pd precursor.

**2.2.2. Bottle around a ship method.** This approach involves the use of pre-synthesized nanoclusters, followed by the addition of MOF precursor (metal nodes and organic linkers) to facilitate the *in situ* growth of the MOF around the nanocluster. The functional group present on the organic linker serves as an anchoring agent, facilitating the uniform distribution of the cluster within the MOF. This approach allows for the encapsulation of larger-size NC in MOFs with smaller pore sizes, thereby accommodating a greater number of clusters. Due to its effectiveness in ensuring the incorporation and stabilization of NC within the MOF's pores, this method is frequently used for synthesis of composite. Zhu *et al.* reported the electrostatic attraction between the negatively charged NC and the positively charged $Zn^{2+}$ metal node assisted in the formation of $Au_{12}Ag_{32}(SR)_{30}$@ZIF-8.[59] This was the first approach in which an oil-soluble, atomically precise NC was incorporated into the MOF through the "bottle-around-the-ship" technique. Other anionic charged nanoclusters like $[Ag_{44}(SR)_{30}]^{4-}$ and $[Ag_{12}Cu_{28}(SR)_{30}]^{4-}$ were incorporated into ZIF-8 MOF using the electrostatic attraction principle and the formation of $Ag_{44}(SR)_{30}$@ZIF-8 and $Ag_{12}Cu_{28}(SR)_{30}$@ZIF-8 nanocomposite were observed. Besides, MOF frameworks like ZIF-67 and MHCF were utilized to synthesize nanocomposite incorporating those anionic clusters. Wu and co-workers reported the encapsulation of the newly synthesized $Au_{38}I(S\text{-}Adm)_{19}$, $Au_{38}S(S\text{-}Adm)_{20}$, and $Au_{38}IS(S\text{-}Adm)_{19}$ NCs in UiO-66-X (where X = –F, –OH, –COOH, –$NH_2$) using "bottom-up construction" of MOF.[70] The authors examined the effects of substituting a single non-metal atom and its impact on optical properties. They asserted that embedding the NC within the MOF resulted in a partial release of -S-Adm protective ligands from the NC, thereby increasing the accessibility of the catalytic surface for enhanced catalytic activity (Fig. 5a). Therefore, the surface engineering of the NC and the modification of the MOF functional groups resulted in tuning the catalytic efficiency of the composite system. Jiang *et al.* encapsulated single heteroatom-doped UiO-66-$NH_2$ MOF analogues of $MAg_{24}$ affording $MAg_{24}$@UiO-66-$NH_2$ (M = Au, Ag, Pt, Pd).[71] The electrostatic attraction between the negatively charged $MAg_{24}$ nanocluster and the positively charged zirconium metal node of the MOF formed the composite. Then the addition of the organic linker allowed forming the MOF around the NC (Fig. 5b). The single hetero-doped nanocomposite systems showed better catalytic activity as compared to $Ag_{25}$@UiO-66-$NH_2$ for photocatalytic hydrogen production. XAS studies and ultrafast studies revealed that the $MAg_{24}$ nanocluster was present inside the MOF, which facilitated the Z scheme charge transfer pathway in the presence of light.

Fischer *et al.* immobilized $[NBu_4]_2[\{Pt_3(CO)_6\}_3]$ NC into ZIF-8 MOF. The encapsulated cluster exhibited sensitivity to oxidation, leading to its transformation into the $[NBu_4]_2[\{Pt_3(CO)_6\}_4]$@ZIF-8 nanocomposite upon exposure to air.[72] The carbonyl groups were stripped off from the cluster by treating the composite at 200 °C for 4 h. Further, the FTIR data confirmed the total loss of CO ligands from the composite system. Further analysis revealed that the platinum clusters were evenly distributed within the MOF without any aggregation. This uniformity is attributed to the confinement effect provided by the MOF. Fischer and coworkers also encapsulated bimetallic Pt(M) (M = Co, Ni, Fe, Sn) clusters in ZIF-8 MOF using the bottle-around-ship approach.[73] Following this, the decarbonylation of the CO ligand that protected the surface of the NC, led to yield of a ligand-free, NC encapsulated within the MOF.

The analysis of cluster size revealed that only the homometallic $Pt_9$ and the bimetallic $Co_8Pt_4$ clusters were successfully encapsulated within the MOF. In contrast, the remaining clusters were located at the edges of the MOF, as their larger sizes and other limiting factors prevented them from being encapsulated inside the MOF's pores. Copper NCs have recently become more significant than gold and silver NCs because of their cost-effectiveness and availability, enabling their large-scale application. Serre *et al.* encapsulated copper NC in zirconium-based MOFs UiO-66-$NH_2$ and MOF-801 using the bottle-around-a-ship strategy.[74] The composite utilized for $CO_2$

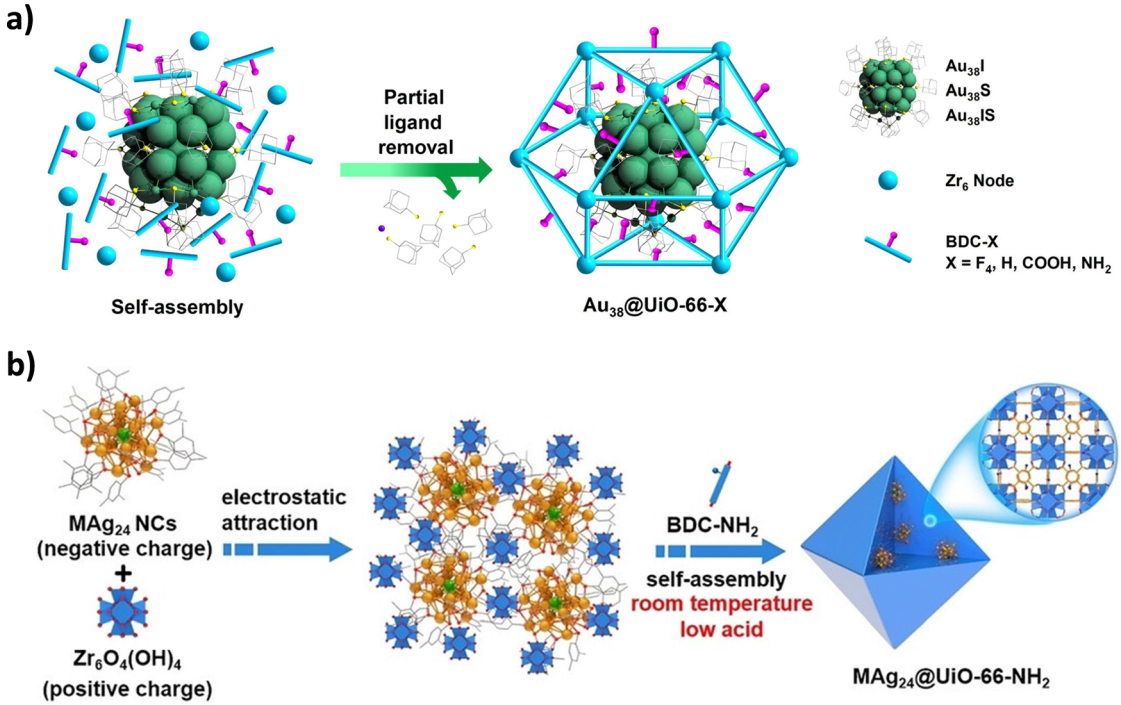


Fig. 5 (a) Schematic illustration of the synthetic route to partial-ligand-removed $Au_{38}$@UiO-66-X composites based on the self-assembly of $Au_{38}$ NCs and UiO-66-X MOF precursors. Reproduced with permission from ref. 70. (b) Schematic illustration showing the synthetic route to $MAg_{24}$@UiO-66-$NH_2$ by encapsulating $MAg_{24}$ clusters into UiO-66-$NH_2$ *via* electrostatic attraction and self-assembly at room temperature under low-acidity conditions. Reproduced with permission from ref. 71.

photoreduction. The mechanistic studies indicated that the stabilized $Cu^I$ at the interface of the encapsulated copper NC and the MOF acted as the active site for catalysis due to a synergistic effect. Steunou *et al.* synthesized $Au_{25}SG_{18}$ NC and encapsulated it into an iron(III) carboxylate MOF MIL-100(Fe).[75] The as-synthesized NC was mixed with the MOF precursors $Fe(NO_3)_3$ and linker trimesic acid to obtain the hybrid material $Au_{25}$@MIL(Fe) at room temperature. Different amounts of NC were taken to prepare $Au_{25}(X)$@MIL-100 ($X$ = 3 to 13 wt%). Among composite systems, the highest loading of NC (*e.g.*, $Au_{25}(13)$@MIL) was investigated for the anti-inflammatory properties of the material.

Jiang *et al.* studied the interaction between the NC and the metal node of the MOF. The composite system was formed based on the coordinated self-assembly and electrostatic interactions, which yielded $Au_{25}$@M-MOF-74 (M = Zn, Ni, Co, Mg).[76] The microenvironment of $Au_{25}(Cys)_{18}$ could be modulated by different metal nodes (Fig. 6). The coordination interactions

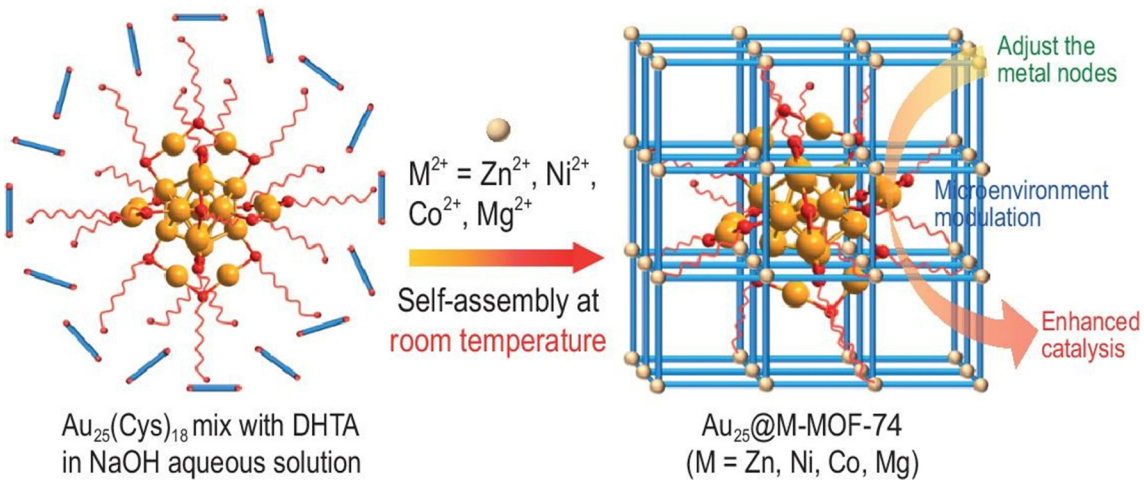


Fig. 6 Schematic illustration showing the synthetic route to $Au_{25}$@M-MOF-74 (M = Zn, Ni, Co, Mg) for enhanced catalysis through microenvironment modulation around $Au_{25}(Cys)_{18}$ by adjusting the metal nodes on MOF pore walls. Reproduced with permission from ref. 76.

 

between the metal–oxo chain in M-MOF-74 and the free carboxyl groups from the surface-bound ligand Cys on $Au_{25}(Cys)_{18}$ effectively reduced the free vibration of the surface ligands on the $Au_{25}$ NC. This modification enhanced the accessibility of the Au sites and resulted in variations in the fluorescence properties of these materials. It was noted that stronger interactions contributed to an increased electron density and core expansion within $Au_{25}(Cys)_{18}$ NC, thereby facilitating catalysis in the following order: $Au_{25}$@Ni-MOF-74 > $Au_{25}$@Co-MOF-74 > $Au_{25}$@Zn-MOF-74 > $Au_{25}$@Mg-MOF-74.

### 2.3. Self-assembly of nanocluster

This technique involves the NC as a metallic node, which is interconnected *via* a ligand present on the surface of the NC. This ligand acts as a bridging agent between two nanocluster units, facilitating their combination into a one-dimensional (1D), two-dimensional (2D), or three-dimensional (3D) framework that forms a cluster-based network similar to that of the MOF system. These materials demonstrated a well-structured and porous characteristic. A prominent example of cluster-based MOFs is the silver chalcogenolate, which utilizes Ag–N interactions to connect the network components. Zang *et al.* demonstrated the inter-nanocluster connection of $Ag_{12}$ NCs $(Ag_{12}(S^tBu)_6(CF_3COO)_6(CH_3CN)_6)$ to form a MOF based on $Ag_{12}$ NC, referred to as $Ag_{12}$bpy. This was achieved by replacing the coordinated $CH_3CN$ ligands in $Ag_{12}$ NC with the linear bidentate linker 4,4′-bipyridine (bpy), resulting in an $Ag_{12}(S^tBu)_8(CF_3COO)_4$-$(bpy)_4$, as illustrated in Fig. 7. In the framework of $Ag_{12}$bpy, each $Ag_{12}$ node is linked to four adjacent nodes *via* eight $\mu^2$-bpy bridges and an open channel with a rectangle cross-section measuring 11.78 × 6.47 Å$^2$.[77] Several other Ag NCs, including $Ag_4$,[78] $Ag_8$,[79] $Ag_{10}$,[80] $Ag_{14}$,[81–84] $Ag_{15}$,[81] $Ag_{18}$,[85] and $Ag_{27}$,[86] have also been synthesized into 2D or 3D cluster-based MOFs using N-containing linkers with different configurations and functionalities. By linking the clusters together, there is a notable increase in the stability of the cluster along with an enhancement in its catalytic capabilities. The ability to adjust the surface ligands of NC enables the customization of linkers, resulting in different cluster assemblies. So far, research has predominantly concentrated on N-based linkers, while some assemblies using S/O-based linkers are also being developed. Dong *et al.* synthesized a series of Ag NC-based MOFs using a triangular, thiourea-based linker, yielding structures TNS-$Ag_8$ and TOS-$Ag_4$. In the TNS-$Ag_8$ framework, the $Ag_8$ cluster functions as a 6-connected node, creating a channel with a cross-sectional area of 9.0 × 9.0 Å$^2$. Similarly, the TOS-$Ag_4$ network features a channel of 10.0 × 10.0 Å$^2$, formed by 3-connected $Ag_4$ nanoclusters.[83]

### 2.4. Synthetic challenges and opportunity

Upon reviewing the different synthesis techniques for NC@MOF composite, it is evident that the *in situ* encapsulation method is more advantageous than the post-synthetic modification approach. This advantage is largely attributed to the critical role of surface anchoring deriving forces such as a covalent bonding—between the MOF and the NC, van der Waals forces, π–π, coordination, and electrostatic interactions. These interactions are essential for maintaining stability, especially in challenging reaction environments, where there is an increased likelihood of NC aggregation or separation from the MOF due to insufficient interaction strength in the absence of a confinement effect. While the effectiveness of post-synthetic modification is influenced by the stability of the pre-synthesized MOF and the subsequent composite formation. A vital step in this process is the activation of the MOF, while the possibility of NC

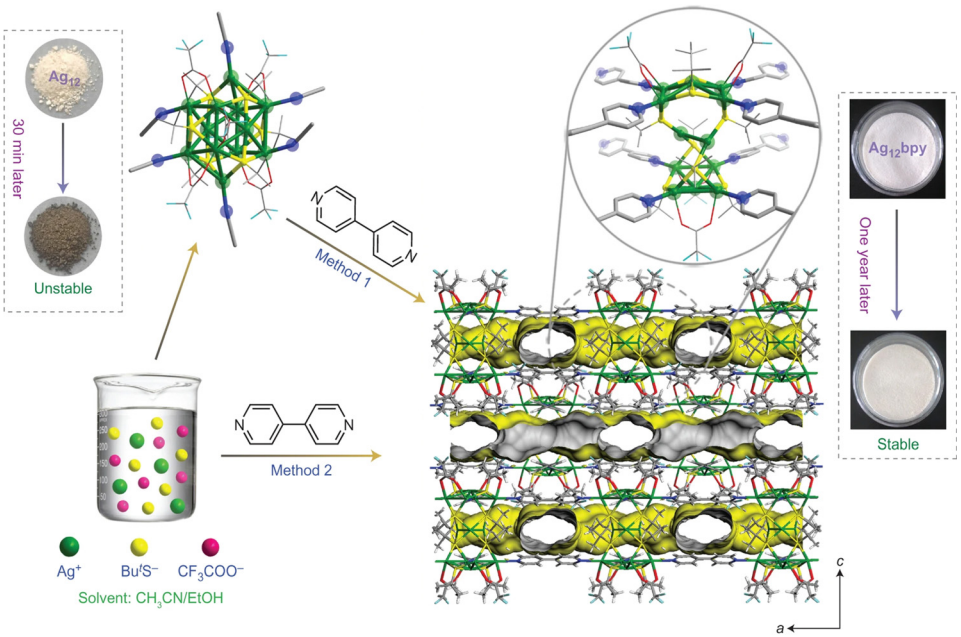


Fig. 7 Schematic illustration of the ligand-exchange strategy (method 1) used to obtain $Ag_{12}$bpy crystals and one-pot synthesis (method 2) under identical conditions. Reproduced with permission from ref. 77.

leaching exists, attributed to weak interactions and size discrepancies within the pore structure. The ''bottle-around-ship'' method (*in situ*) effectively reduces leaching, ensures a consistent distribution, and optimizes the stabilization of the embedded clusters. Besides, the ''ship-in-a-bottle approach'', presents significant challenges. To achieve precise NC within MOF, it is essential to implement a rigorously controlled kinetic process during the reduction phase, followed by a size-focusing step or a purification procedure. This approach raises concerns during the *in situ* formation of clusters within the MOF, as impurities might be trapped in the framework, which could negatively affect the catalytic performance of the composite system. In addition, there is a limitation on the size of NC that can be integrated into MOF, as the growth of the NC is influenced by the pore size of the MOF due to *in situ* formation. The self-assembly of NCs into a cluster-based framework demonstrates a significant advantage in structural manipulation and the tailoring of NC properties. This technique not only promotes enhanced stabilization but also enables the fusion of functionalities between NCs and MOFs. However, a notable limitation is that the bridging linkers available for the construction of cluster-based MOFs are predominantly restricted to nitrogen-donor ligands. Although the research has been conducted on sulfur and oxygen-based linkers. The materials synthesized from these alternatives are limited. Thus, there is a compelling need for the introduction of novel bridging linkers or new bonding modes of cluster-based MOFs. The importance of including the NC in the MOF is noted for its role in manipulating the microenvironment. This could be achieved by changing the NC ligand functional group or MOF pore engineering. For example, the ligands on the NC entrapped inside the MOF could be stripped off under thermal conditions to yield a surface-clean NC. This exposes the active sites, reducing steric hindrance from the ligands, and allowing easier access for incoming reactant molecules, which enhances catalytic activity. Additionally, the MOF's confinement effect prevents NC aggregation, even after ligand removal, ensuring stability and maintaining catalytic efficiency. The functional group present on the organic linker can further modulate the stability and catalytic activity of the entrapped NC. Jiang *et al.* reported a nanocomposite system, in which they regulated the microenvironment around the $Au_{25}$ nanocluster using the confinement effect of the MOF.[87] Utilizing electrostatic attraction and coordination interactions, the pre-synthesized $Au_{25}(Capt)_{18}$ was successfully encapsulated in the pores of UiO-66-X (X = $-NH_2$, –OH, –H, $-NO_2$) as illustrated in Fig. 8a. Following this, the composite system underwent a thermal treatment at 275 °C to remove the surface-protecting ligands from the NC, yielding a surface-clean $Au_{25}$ NC within the MOF structure. The surface-clean $Au_{25}$ NC, confined within the MOF structure, demonstrates significantly enhanced activity and stability compared to pristine $Au_{25}$ nanoclusters in the oxidative esterification of furfural. Zhao *et al.* recently used a rigid γ-cyclodextrin MOF (γ-CD-MOF) with sufficiently large cavities to host the ligands of NCs ($Au_{40}(Adm)_{22}$) *via* host–guest chemistry. Once anchored onto the γ-CD-MOF surface, each NC ($Au_{40}(Adm)_{22}$) is enclosed by the γ-CD molecules, thereby stabilizing the ligands. This stabilization restricts ligand movement, allowing reactants to interact readily with the exposed metal surface of the $Au_{40}$ NCs through the gaps created by the rigidified ligands (Fig. 8b). Therefore, in a horseradish peroxidase-mimicking reaction, $Au_{40}$/γ-CD-MOF demonstrated significantly enhanced catalytic activity compared to unmodified $Au_{40}$ NCs. This approach is versatile and can also be applied to other NCs with distinct ligands, such as $Au_{38}(PET)_{24}$ and $Au_{44}(2,4\text{-DMBT})_{26}$.[88]

### 2.5. Structural integrity MOFs and NCs

It is of considerable interest to the researcher to maintain the well-defined architecture and chemical functionality of MOF during composite (*e.g.*, NC@MOF) formation with NC guests. The unique characteristics of MOF matrices serve to prevent the aggregation of NC during heterogeneous catalysis, granting them notable features like the molecular sieving effect.[89,90] However, the effectiveness of surface anchoring is diminished due to the weak nature of host–guest interactions (coordinative, electrostatic, *etc.*). Moreover, it becomes increasingly challenging to regulate NC aggregation in harsh environments, particularly at elevated temperatures. Unlike surface anchoring,

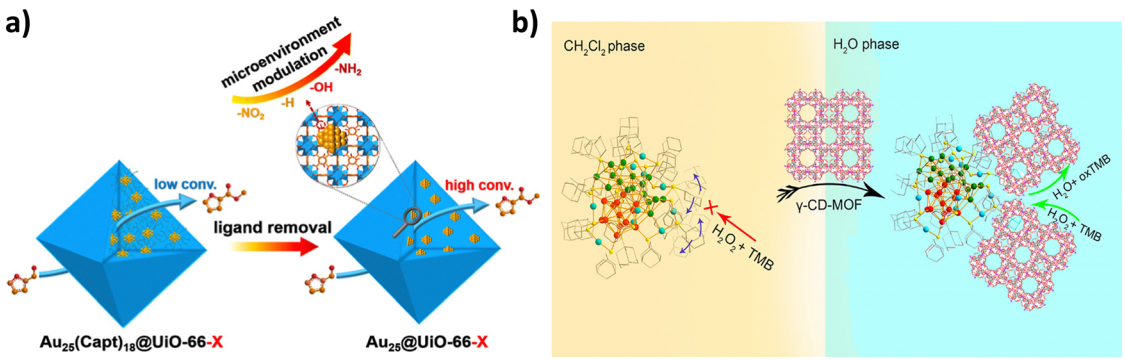


Fig. 8 (a) Schematic illustration showing the synthetic route to $Au_{25}(Capt)_{18}$@UiO-66-X to surface clean $Au_{25}$@UiO-66-X for enhanced catalysis through microenvironment modulation around $Au_{25}$ by adjusting the functional group on linker of MOF pore walls. Reproduced with permission from ref. 87. (b) Schematic illustration showing the encapsulation of $Au_{40}(S\text{-}Adm)_{22}$ by γ-CD-MOF to form $Au_{40}$/γ-CD-MOF for phase transfer and enhanced catalysis in horseradish peroxidase reaction. Reproduced with permission from ref. 88.

 

pore-confined growth can effectively limit agglomeration and leaching. Additionally, since the NCs are physically situated within the MOF pores, aggregation can be mitigated even at elevated temperatures. However, this approach may face challenges in achieving the desired atomic precision of NCs due to the limited pore size of the MOF. Maintaining atomic precision during the reduction phase, along with subsequent size-focusing, kinetic control, and separation processes, presents difficulties. Therefore, the *in situ* encapsulation offers a potential solution to these challenges. This approach allows for the encapsulation of NC of various shapes and sizes within MOF. The MOF serves as a protective shell, preventing the migration and aggregation of the NC. Furthermore, the structural integrity of the MOF's pores is maintained, as it depends on the surface of the NC to facilitate interactions with external analytes for reactions. This method incorporates strategies such as coordination-assisted self-assembly and electrostatic attraction. For instance, $Au_{25}(SG)_{18}$ is encapsulated into ZIF-8, and the coordinating interaction between $Zn^{2+}$ and the –COOH functional group of the SG ligand boosts the self-assembly of ZIF-8.[62] Further examples can be found in the electrostatic technique, where the ionic NC (*e.g.*, $[Au_{12}Ag_{32}(SR)_{30}]^{4-}$) is mixed with a $Zn^{2+}$ solution containing a linker (*e.g.*, 2-methylimidazole) to enable controlled encapsulation within ZIF-8 scaffolds.[59] It is crucial to emphasize that the negatively charged NC and the positively charged metal node (*e.g.*, $Zn^{2+}$) were the fundamental driving forces for the composite formation. Therefore, with a strategic selection of NC and MOF, electrostatic attraction-assisted encapsulation offers greater versatility, accommodating a diverse range of NC shapes and sizes (*e.g.*, $Ag_{44}$, $Ag_{12}Cu_{28}$) within the frameworks (*e.g.*, ZIF-8, ZIF-67, *etc.*). Notably, this method is particularly advantageous when conducted at room temperature, allowing for the utilization of temperature-sensitive MOFs. By employing this strategy, it is possible to successfully encapsulate NCs while maintaining the intrinsic properties and structural integrity of both the MOFs and the NCs.

## 3. Composite characterization methods

The composites are analyzed using a range of advanced, cutting-edge analytical and spectroscopic techniques to gain comprehensive insights into their structure and properties. A deep understanding of the material is essential and envisioned for developing new methods for potential applications. In-depth characterization of composites not only facilitates a better understanding of their properties and potential uses but also enhances the optimization of synthesis techniques, which is fundamental to the progress of this field of study. The characterization of NC@MOF composite often considered to be challenging, as they are complex inorganic–organic hybrid materials. To obtain a comprehensive view of the structure and properties of the composites, information on their crystallinity, porosity, composition, *etc.*, are collected using multiple spectroscopic and microscopic tools. The ultra-small size of the NCs renders their analysis within the composite particularly challenging, leading to the strategic utilization of novel analytical methods to effectively tackle this problem. Inductively coupled plasma (ICP) spectroscopy plays a crucial role in determining the composition of the composite. By utilizing ICP, the metal contents are measured with high accuracy, facilitating a quantitative confirmation of the incorporation of NCs.[70,87] Powder XRD is one of the preliminary techniques that is used to characterize the NC@MOF composite. It gives information regarding the crystallinity and the phase purity of the material. There are instances in the synthesis of the composite; the crystallinity of the MOF could be compromised, like the agglomeration of NCs and problems in the MOF formation because of the presence of NCs in the bottle-around-the-ship approach, *etc.* A good match between the PXRD of the intact MOF and the composite is always an indication of the formation of a stable composite. The shift in peak position and variation in intensity observed in the composite, resulting from the interaction between the NC and MOF, also offer valuable insights. Zhu *et al.* incorporated $Au_{25}$(L-Cys)$_{18}$ and $Au_{25}(PET)_{18}$ in UiO-66-$NH_2$ MOF, and they observed that the PXRD patterns of the MOF remained unchanged after the incorporation of the Au NCs, indicating the intact crystallinity of the MOF (Fig. 9a).[60] Also, because of the ultrasmall size of the NC, there were no diffraction peaks associated with Au NCs. UV-vis spectroscopic analysis is a very powerful technique for the characterization of NC@MOF composites. It could reveal very crucial information, like the stability of the cluster in the composite and the interaction between NC and MOF, which is pivotal in understanding these hybrid materials. Wu *et al.* used UV-vis/NIR spectroscopic studies in their work to confirm the structural integrity of the NC after incorporation in MOF, where they constructed UiO-66 MOF around $Au_{38}$ NCs in a bottom-up manner.[70] Wang *et al.* also conducted UV-vis spectroscopic studies on their $MAg_{24}$@UiO-66-$NH_2$ (M = Ag, Pd, Pt, and Au) composite and observed the characteristic peaks of the synthesized cluster (Fig. 9b and c).[71] The Fourier transform-infrared (FT-IR) spectroscopy is essential for characterization, as it offers valuable information regarding the interactions between NCs and MOFs. FT-IR spectra of the material could provide insights into the functional groups present in the composite, bonding interactions within the composite, and the incorporation of NCs. Yun *et al.* used FT-IR to investigate the –COO– functional group interaction of NC ($Au_{25}$) ligand with $Zn^{2+}$ or $Co^{2+}$ ions in the ZIF-8, ZIF-67 MOFs, and ZIF-8@$Au_{25}$@ZIF-67 composites, respectively.[63] A new peak emerged at 520 $cm^{-1}$, which was attributed to the Zn–O or Co–O stretching vibration, corresponding to the Au-Cys-Co or Au-Cys-Zn linkage. The porosity of the MOF is an interesting feature to study before and after the NC incorporation with MOF. This could provide information for the type of composite, comparative loading of NCs, *etc.* Typically, the surface area decreases upon the encapsulation of NC due to the pore's occupancy. In addition, it could also help in differentiating the surface-bound NC (*e.g.*, NC/MOF) or encapsulated within the pore matrices of MOF. Wang *et al.* found that

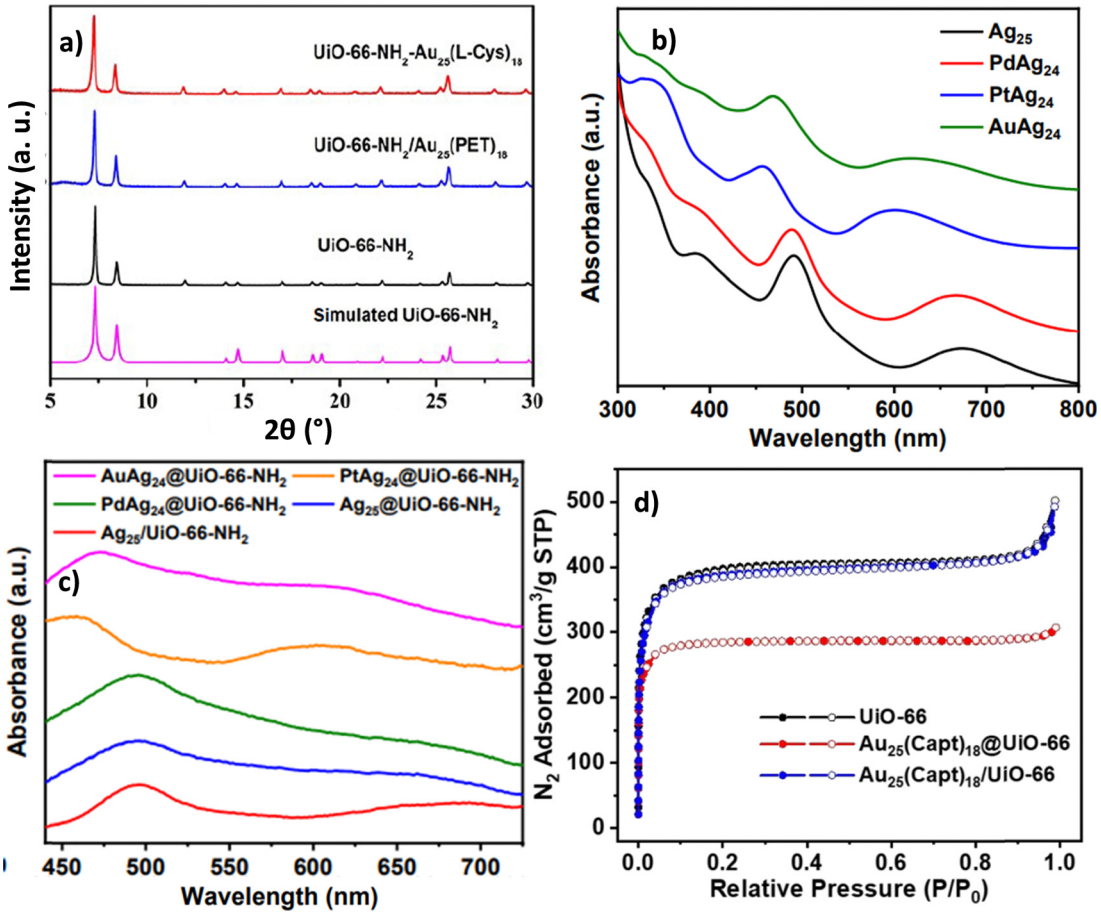


Fig. 9 (a) XRD patterns of UiO-66-$NH_2$-$Au_{25}$(L-Cys)$_{18}$, UiO-66-$NH_2$/$Au_{25}$(PET)$_{18}$, and UiO-66-$NH_2$ (simulated and experimental). Reproduced with permission from ref. 93. (b) UV-vis spectra of $MAg_{24}$ (M = Ag, Pd, Pt, and Au) in $CH_2Cl_2$ solvent. (c) UV-vis spectra of $MAg_{24}$ NCs loaded on or encapsulated into UiO-66-$NH_2$ by subtracting the spectrum of UiO-66-$NH_2$ from $Ag_{25}$/UiO-66-$NH_2$ and $MAg_{24}$@UiO-66-$NH_2$. Reproduced with permission from ref. 71. (d) $N_2$ sorption isotherms of UiO-66, $Au_{25}(Capt)_{18}$@UiO-66, and $Au_{25}(Capt)_{18}$@UiO-66 at 77 K. Reproduced with permission from ref. 87.

the surface area of the $Au_{25}$@UiO-66 (853 $m^2\ g^{-1}$) was comparatively lower than surface anchored NC ($Au_{25}$/UiO-66, 1174 $m^2\ g^{-1}$) (Fig. 9d).[87] The findings indicated that the pore space of UiO-66 is occupied by $Au_{25}(Capt)_{18}$, resulting in the formation of $Au_{25}(Capt)_{18}$@UiO-66. Conversely, $Au_{25}(Capt)_{18}$ may remain on the surface of the MOF in the case of $Au_{25}(Capt)_{18}$/UiO-66. X-ray photoelectron spectroscopy (XPS) is an essential technique for investigating the electronic structure, elemental composition, and chemical state of NC@MOF composites. It primarily helps to identify the oxidation states of the elements within the composite. Additionally, XPS can provide insights into the interactions between NC and MOF. Su *et al.* employed XPS analysis to investigate the oxidation state of Au in $Au_{25}$@ZIF-8 composite (Fig. 10a and c).[62] $Au_{25}(SG)_{18}$-ZIF-8 nanocomposite shows a minor negative shift in the Au $4f_{7/2}$ peak (83.7 eV) compared to $Au_{25}(SG)_{18}$ (84.1 eV).[91] This result indicates that the formation of negatively charged $Au_{25}$ clusters occurs after the encapsulation of $Au_{25}(SG)_{18}$ within ZIF-8, presumably due to interactions with ZIF-8. *In situ* XPS experiments are also emerging tool in the field of composite materials characterization. Kratzl *et al.* used *in situ* XPS analysis to study the formation of $Pt_{12\pm x}$NC@ZIF-8 composites by the thermal decarbonylation of $[NBu_4]_2[\{Pt_3(CO)_6\}_4]$@ZIF-8 at 200 °C for 3 h.[72] The binding energy peak of Pt $4f_{7/2}$ was found to be 71.1 eV, which is close to the reported value for decarbonylated Pt NCs. Signals for N 1s and Zn 2p match with the ZIF-8 MOF. X-ray absorption spectroscopy (XAS) is employed for studying the local atomic structure of the material and its coordination environment. XAS also provides the interaction between the NC and the MOF. Fischer *et al.* used XAS to study their system, where carbonyl-protected NCs ($Co_8Pt_4$) were incorporated in ZIF-8 (Fig. 10d).[92] From XANES analysis, they could observe that the Co got oxidized further upon the incorporation into the MOF. This could be attributed to the interaction between MOF-matrices, partial removal of CO ligands, and damage caused by X-ray beams. EXAFS studies showed that $d_{Co-Co}$ decreased by 0.1 Å in the encapsulated $Co_8Pt_4$ as the cluster is located within the micropores of the framework. Microscopic analyses are crucial for investigating NC@MOF composite materials, as they offer insights into the size distribution of NCs. The TEM images analysis, such as high-angle annular dark field scanning (HAADF-STEM) and bright-field (BF-TEM) is curial for investigation. The TEM-energy dispersive X-ray spectroscopy (EDS), TEM-electron energy loss spectroscopy (EELS) along with elemental mapping are excellent for elemental analysis of the composite material. Jiang *et al.* used

 

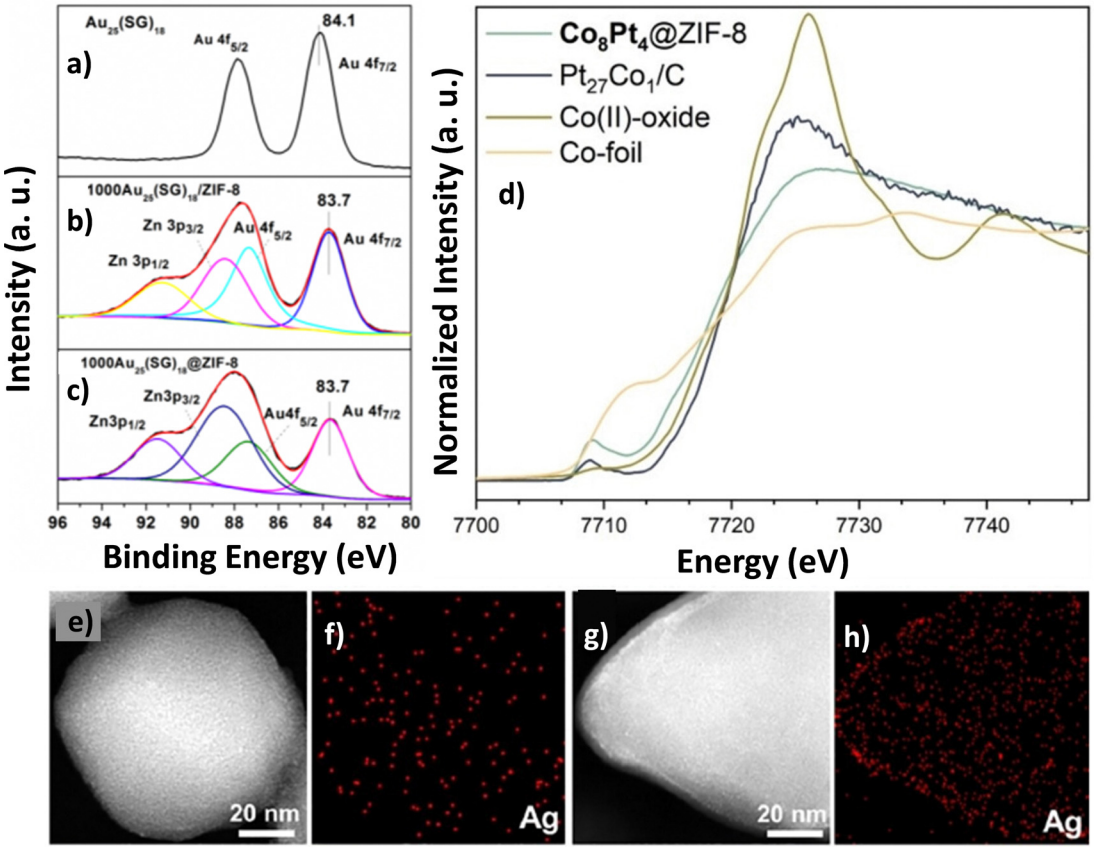


Fig. 10 XPS spectra of (a) $Au_{25}(SG)_{18}$, (b) $1000Au_{25}(SG)_{18}$/ZIF-8 and (c) $1000Au_{25}(SG)_{18}$@ZIF-8 from Au 4f and Zn 3p. Reproduced with permission from ref. 62. (d) Co Kα HERFD XANES of $Co_8Pt_4$@ZIF-8 and $Pt_{27}Co_1$/C. The XANES of Co(II)-oxide and Co-foil are also shown for comparison. Reproduced with permission from ref. 92. (e) and (f) HAADF-STEM images and the corresponding EDS mapping of Ag for $Ag_{25}$@UiO-66-$NH_2$ and (g) and (h) $Ag_{25}$/UiO-66-$NH_2$. Reproduced with permission from ref. 71.

the HAADF-TEM to visualize and compare $Ag_{25}$@UiO-66-$NH_2$ and $Ag_{25}$/UiO-66-$NH_2$ (Fig. 10e and h).[71] The careful analysis of the images revealed that the $Ag_{25}$ NCs were incorporated into the pores of the MOF ($Ag_{25}$@UiO-66-$NH_2$) while other ($Ag_{25}$/UiO-66-$NH_2$) distributed over the surfaces. TEM-EDS analysis indicated the presence of uniformly distributed NCs all over the MOF in the case of $Ag_{25}$@UiO-66-$NH_2$. Whereas the Ag NCs were found to be occupying the edges of the MOF in $Ag_{25}$/UiO-66-$NH_2$.

## 4. Catalytic performance of the nanocomposite

Since MOFs have been shown unprecedented properties and fine-tuning of liker and metal nodes provide the interactive host for the NC guest. The mutual support of MOF/NC not only retains the stability; however, approaches enhance catalytic efficiency for a variety of reactions.[50,94] In addition, ultrasmall size, high surface area, known crystal structure, and active site warrant a comprehensive understanding of the mechanism. Here, we summarise the key factors that affect the reactivity efficiency and site selectivity for (a) photocatalysis and (b) value-added small molecule transformation.

### 4.1. NC@MOF assisted photocatalysis

There are a plethora of reports and comprehensive reviews available for the immobilization of nanoparticles with the MOF and employed for photocatalytic application.[47,48,93,95,96] However, NC@MOF composite has shown distinctive properties and selectivity for environmental photocatalysis (*e.g.*, $CO_2$ reduction). Fei *et al.* have reported ultrafine gold (Au) NC (Au-NC@UiO-68-NHC) composite for photochemical $CO_2$ reduction.[67] The Au NCs were stabilized by N-heterocyclic carbenes (NHCs) functionalized UiO-68-NHC pore matrices. The covalent bonding bridge between MOF-NHC-Au helps in modulating the reaction with precise control over the reaction mixtures. The composite afforded the yield of 57.6 μmol $g^{-1}$ $h^{-1}$ for $CO_2$ to CO formation, which is four times higher than the UiO-68-$NH_2$/Au.

In addition, the comparative studies reveal that the Au-NC@UiO-68-NHC have a higher rate of CO production than MOF and UiO-68-$NH_2$/Au mixture (Fig. 11a). The prepared catalyst was stable for up to 3 cycles and retains a reduction efficiency of up to 90 to 95% (Fig. 11b). The energy of the highest occupied molecular orbital (HOMO) and lowest unoccupied molecular orbital (LUMO) of Au-NCs were estimated to be 1.71 V and 0.43 V, suggesting the transfer of excited state electrons from Au-NCs to UiO-68 *via* Au-NHC bridges (Fig. 11c).

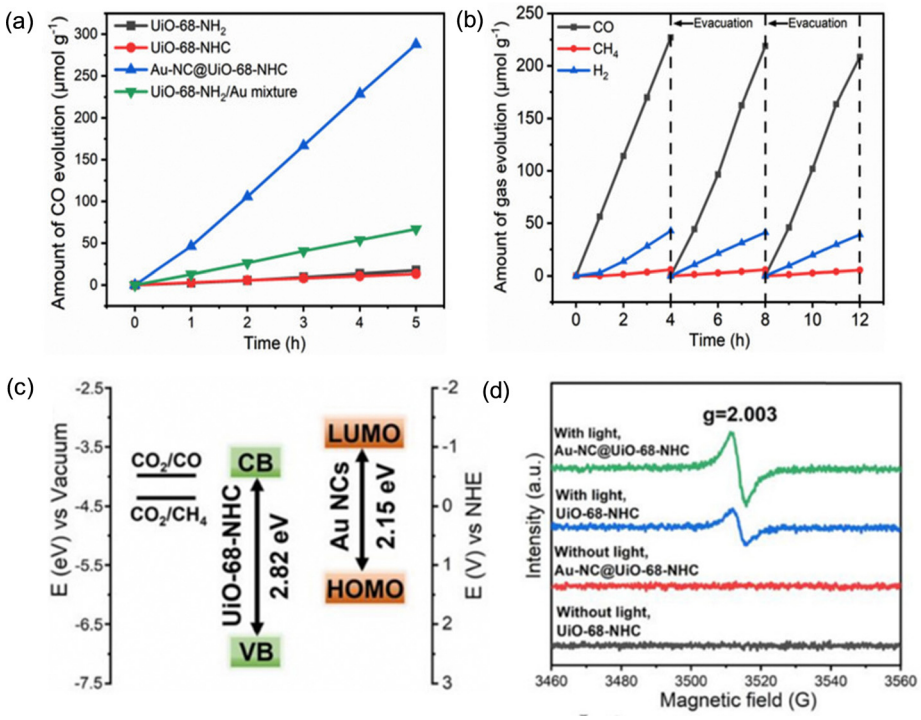


Fig. 11 (a) Time courses of CO evolution by photocatalytic $CO_2$ reduction using UiO-68-NHC, Au-NC@UiO-68-NHC, UiO-68-$NH_2$, and Au/UiO-66-$NH_2$ as photocatalysts upon AM 1.5G irradiation. (b) Time courses of photocatalytic $CO_2$ reduction on Au-NC@UiO-68-NHC under AM 1.5G irradiation for 12 h, with evacuation every 4 h. (c) Band alignment of Au NCs and UiO-68-NHC. (d) ESR spectra of UiO-68-NHC and Au-NC@UiO-68-NHC with light and/or without light. Reproduced with permission from ref. 67.

Furthermore, the EPR signals is an evidence of the generation of $Zr^{3+}$ species upon irradiation where Au-NCs facilitate the electron transfer (Fig. 11d). Authors proposed that the catalytic active site is found to be $Zr^{3+}$ for the $CO_2$ to CO conversion. Serre *et al.* reported Cu NCs@MOFs core–shell composite for $CO_2$ photoreduction[74] The photochemical $CO_2$ reduction was performed under UV irradiation (385 nm), which yielded HCOOH (64.9%, 94 μmol $h^{-1}$ $g^{-1}$) as a major product along with CO (22.5%, 32 μmol $h^{-1}$ $g^{-1}$) as a minor (Fig. 12a and b). It was found that Cu NCs@UiO-66-$NH_2$ showed better performance with an

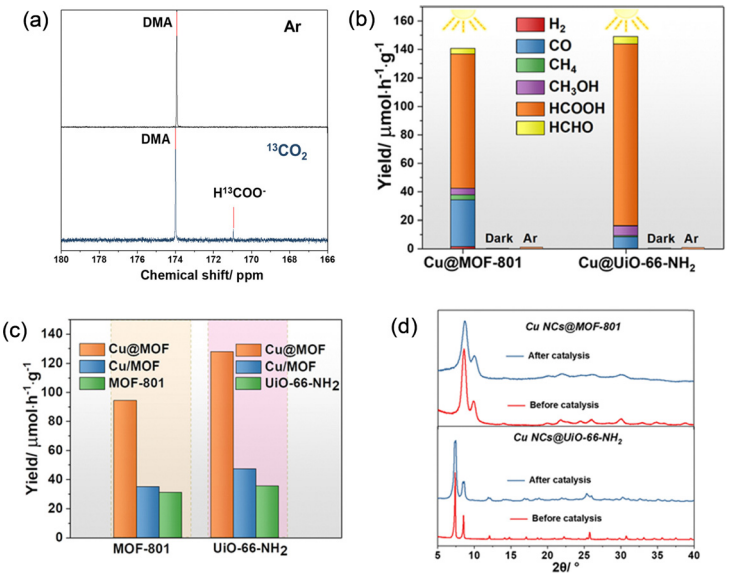


Fig. 12 (a) $^{13}C$ NMR spectra of the photocatalysis products under Ar and $^{13}CO_2$ gas feeding. (b) Production of the photocatalyzed $CO_2$ with Cu NCs@MOF-801 and Cu NCs@UiO-66-$NH_2$ compared to the corresponding blank experiments. (c) Comparative rates of HCOOH formation with Cu/MOFs, and core–shell CuNCs@MOFs. (d) PXRD patterns of Cu NCs@MOF-801 and Cu NCs@UiO-66-$NH_2$ before and after photocatalysis. Reproduced with permission from ref. 74.

 

enhanced rate 128 (μmol $h^{-1}$ $g^{-1}$) for formic acid production (Fig. 12c). This is due to the more $CO_2$ uptake driven by the $NH_2$ functional group and strong host–guest interaction (Fig. 12d). Other examples, Xiong *et al.* have reported the encapsulation (*in situ*) of $Au_{25}$(*p*-MBA)$_{18}$ (*p*-MBA = 4-mercaptobenzoic acid) nanocluster into $Cu_3(BTC)_2$ (BTC = benzene-1,3,5-tricarboxylate) MOF.[97]

The composite ($Au_{25}$@Cu-BTC) has shown excellent activity for $CO_2$ photoreduction to CO (Fig. 13a). The structure of *p*-MBA and BTC is anticipated to be similar, where the carboxyl group interacts with the Cu node, facilitating the transfer of electrons from the Au NC to the Cu site. The current density of the composite is 4 times higher than $Au_{25}$/Cu-BTC and 8 times for bare $Cu_3(BTC)_2$ suggesting the excellent photogenerated charge separation (Fig. 13c). The authors observed that the strong interaction of Au NCs and Cu site promoting charge transfer and well-matched size shows the confinement effect.

In addition, Au helps in charge transfer while MOF is for $CO_2$ uptake over the surface (Fig. 13b). Thus the composite performance has increased in comparison to Au NCs and MOF. Horcajada *et al.* have synthesized AgNC@MIL-125-$NH_2$ composite and applied for hydrogenation reaction for *p*-nitroaniline (4-NA) to *p*-phenylenediamine (PPD).[68] In addition, the composite was also investigated for the degradation of methylene blue (MB-dye) and sulfamethazine (SMT-antibiotic). They have achieved 100% transformation for *p*-nitroaniline and 92% and 96% for MB and SMT. This effect was attributed to the enhanced stability of Ag NC upon encapsulation, enabling the charge transfer process on the heterogeneous surface.

**4.1.1. Organic transformation reaction/hydrogenation.** Utilizing heterogeneous catalysts for organic transformations is recognized as an energy-efficient approach and is perceived as the most effective and environmentally sustainable way to achieve atomic economy. Significant progress has been made in this field through the application of nanoparticles, heterostructures, and doping strategies.[93] However, NC composites-assisted catalysis is currently limited but increasingly explored research domain. To promote sustainable environmental development and mitigate irreversible damage, it is essential to rational design of catalysts that are effective, selective, and enduring. Liu *et al.* synthesized the $Au_{11}$:$PPh_3$@ZIF-8 and $Au_{13}Ag_{12}$:$PPh_3$@MIL-101 and used them for the benzyl alcohol oxidation.[66] The $PPh_3$ ligand was strategically removed by controlling the temperature. The bare NCs, which were stabilized by MOFs (MIL-101) have shown enhanced activity and selectivity. It should be pointed out that well-dispersed ultrafine Au NC avails the more catalytic active site while MOFs provide the support for NCs stabilization and surface interaction of reactant molecules. Fischer *et al.* have reported $[NBu_4]_2[\{Pt_3(CO)_6\}_4]$@ZIF-8 composite and applied for the hydrogenation of 1-hexane.[72] ZIF-8 plays a vital role in stabilizing the NC when the ligand is removed. The authors demonstrated that precisely controlled decarbonylation of synthesized $[NBu_4]_2[\{Pt_3(CO)_6\}_4]$@ZIF-8 gets converted to PtNC@ZIF-8 (4). The ligand-free NCs stabilized by the MOF and capable of full conversion of hexane in 3 h with TOF approximately 2000 $h^{-1}$. This enhanced activity is due to the abundant availability of NC active sites while others have shown a sluggish response (Fig. 14).

It is understood that the judicial choice of metal NCs and MOF hosts is important to bring selectivity and enhance catalytic activity. Notably, controlling ligand removal of NCs,

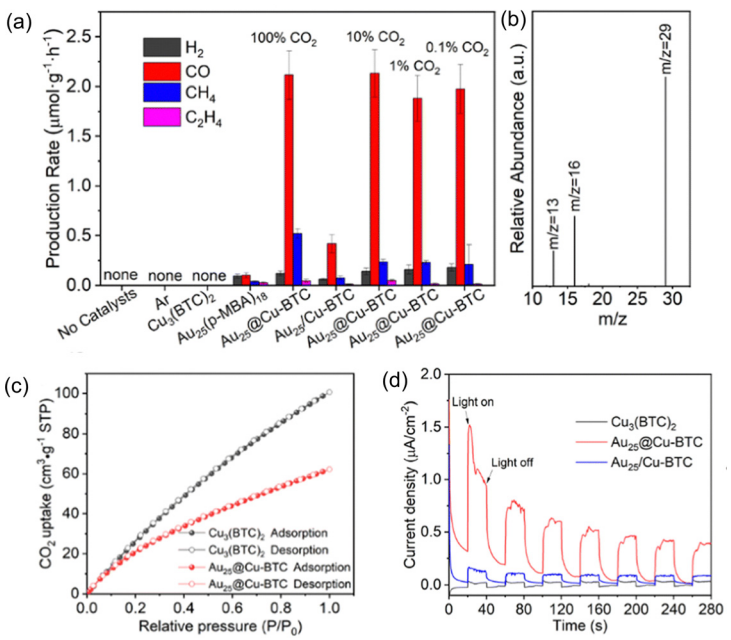


Fig. 13 (a) Average production rates of $H_2$, CO, $CH_4$, and $C_2H_4$ in photoreduction $CO_2$ by $Au_{25}$@Cu-BTC in the first 2 h under visible-light ($\lambda > 420$ nm) irradiation, in comparison with those by $Cu_3(BTC)_2$, $Au_{25}$(*p*-MBA)$_{18}$, $Au_{25}$/Cu-BTC and other control experiments under the same conditions. (b) GC-MS analysis of $^{13}CO$ ($m/z$ = 29) produced over $Au_{25}$@Cu-BTC in light-driven reduction of $^{13}CO_2$. (c) $CO_2$ adsorption behavior for $Au_{25}$@Cu-BTC and bare $Cu_3(BTC)_2$. (d) Transient photocurrent density. Reproduced with permission from ref. 97.

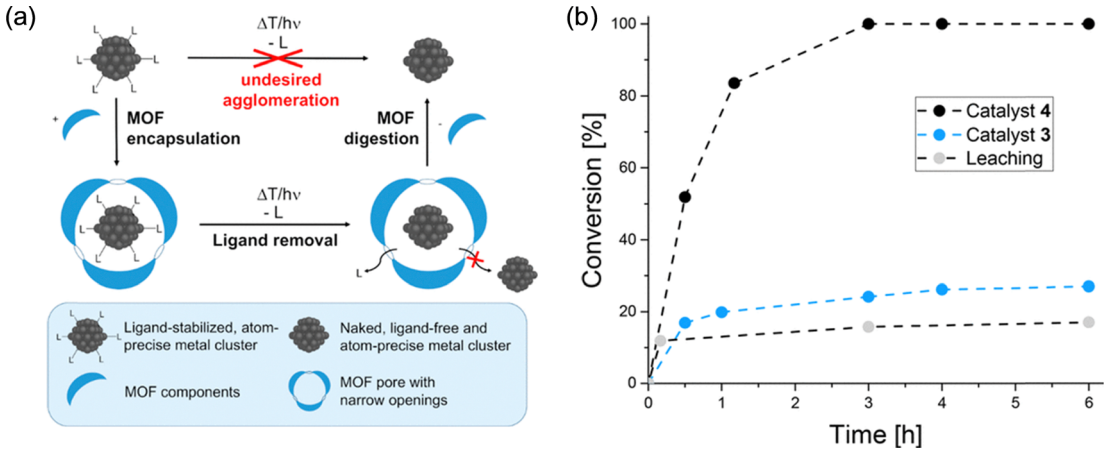


Fig. 14 (a) General concept for the synthesis of ligand-free, atom-precise metal clusters and ultrasmall metal nanoparticles, based on the encapsulation of ligated metal clusters into size-matching pores of metal–organic frameworks chosen as removable protective matrix (b) catalytic hydrogenation of 1-hexene with $[NBu_4]_2[\{Pt_3(CO)_6\}_4]$@ZIF-8 (3) and $Pt_{12\pm x}$@ZIF-8 (4) as catalysts. While with 4, complete conversion is reached after 3 h, the ligand-stabilized clusters in 3 show a significantly slower conversion toward a steady state. When the catalyst 4 is separated after 10 min in a hot filtration experiment, only minimal further conversion is observed, presumably due to Pt species in the solution. Reproduced with permission from ref. 72.

which exceedingly helps for the encapsulation inside MOF's pore matrices leads to chemically and thermally stable and robust composite. Yun *et al.* reported sandwich composites ZIF-8@$Au_{25}$@ZIF-67[tkn] and ZIF-8@$Au_{25}$@ZIF-8[tkn] [tkn = thickness of shell] and investigated for the nitrophenol reduction and terminal alkyne carboxylation with $CO_2$.[63]

ZIF-8@$Au_{25}$@ZIF-67 has shown excellent yield (99%) for the carboxylation of the terminal alkyne using $CO_2$. While bare NCs and MOF (ZIF-8, ZIF-8@ZIF-67) were less efficient and afforded only 10.8%, 27.9%, and 52.3% yields, respectively (Fig. 15a). The findings and observation revealed that the shell thickness and stable NC play an important role in providing the catalytic active site and assisting the substrate interaction for reaction (Fig. 15b). Besides the catalyst was stable up to more than three cycles. The mechanistic investigation suggests that the intermediate bond between an alkyne and an Au center is taking place (Fig. 15c). These studies unveil that encapsulation of NCs in the MOF matrices with the precise tuning of NCs's ligands stabilizing with MOF may give the desired catalytic active site for the selective products. Huang *et al.* reported palladium nanocluster and UiO-66-$NH_2$ composite (Pd@UiO-66-$NH_2$) and employed for the tandem oxidation reaction.[98] Authors reported 99.9% acetal selective for conversion of benzyl alcohol in a single pot tandem reaction of benzyl alcohol and ethylene glycol. The Pd loading significantly modulates the conversion efficiency (1.0, 2.0, and 4.0 wt%). Higher Pd loading resulted in a high yield. The result suggests that palladium is an active site for catalytic conversion and is stable for up to more than 5 cycles in Pd@UiO-66-$NH_2$. While Pd@UiO-66 shows the leaching. Overall, this affects the performance and

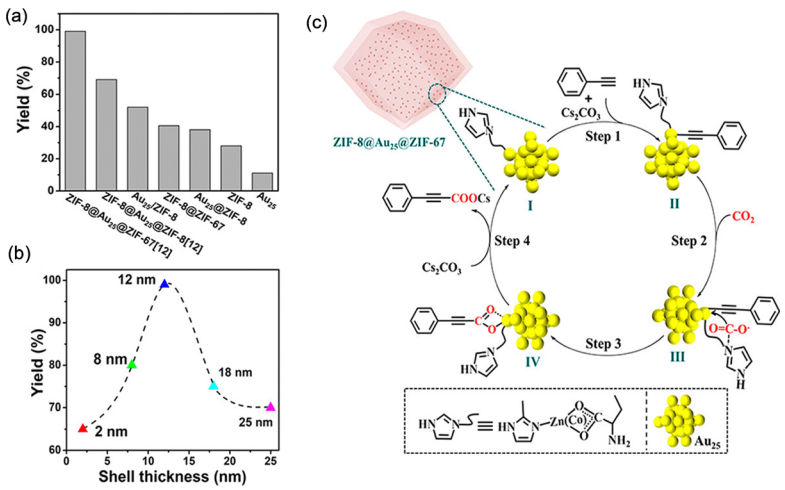


Fig. 15 (a) Catalytic activity of various catalysts for the carboxylation of phenylacetylene. Reaction conditions: catalyst ($1.12 \times 10^{-4}$ mmol of $Au_{25}$), alkyne (0.5 mmol), $Cs_2CO_3$ (0.24 mmol), $CO_2$ (1.0 bar), 50 °C, 12 h. (b) Broken line diagram of catalytic performance of ZIF-8@$Au_{25}$@ZIF-67 with various shell thicknesses. (c) Proposed catalytic mechanism of the reaction between terminal alkynes and $CO_2$ over ZIF-8@$Au_{25}$@ZIF-67[tkn]. Reproduced with permission from ref. 63.

 

diminishes the efficiency. The UiO-66-$NH_2$ was recognized as an effective to enhance the stability of Pd NC.

## 5. Conclusions and outlook

In this feature article, we reviewed the recent development of NCs@MOF composite and catalysis with a particular focus on the choice of MOF and ligand of NCs. MOF has shown unprecedented properties and characteristics for gas absorption and catalysis due to its porous nature and polymeric framework. There has been tremendous progress achieved in making the composite of MOF with other support materials *e.g.*, nanoparticles. However, finding suitable composite materials for catalysis is still being investigated due to functional heterogeneous surfaces and multiple sites for reagent interaction, which complicates analysis. NCs are known to be ligand-stabilized and have well-defined structures, which significantly aid the advantage of establishing host–guest interaction and reactant. In addition, the synergy of NC and MOF composite can significantly influence the electronic structure of NC and heterogeneous surface contributing to boosting the catalytic efficiency. The progress achieved in this field underscores the importance of a new class of functional material and fine-tuning intrinsic properties and mutability. Furthermore, NCs unique properties provide the avenue for the rational design of new composite materials. Various synthetic techniques have been developed for NC@MOF composite preparation. We have outlined and classified these techniques into three main types: (a) post-synthetic modification (b) *in situ* encapsulation, and self-assembly of nanocluster. Furthermore, they are categorized into two subdivisions, which include surface anchoring, solution impregnation, the ''ship-in-a-bottle'', and the ''bottle-around-a-ship'' method. Post-synthetic modification can show the leaching while dispersing in the solution phase. Besides the stability of NCs over the surface is a notable concern. The interaction between NCs' ligand and MOF linker is difficult to analyze due to random distribution over the surface. *In situ* encapsulation is a popular technique substantiating the NCs embedded into the pore matrices. Among those methods, the bottle-around-a-ship is promising due to the scope for the NCs ligand and MOF linker modification. Due to its ultrasmall size (NCs), and low loading, difficult to identify through PXRD. However, the microscopic technique like HRTEM is frequently being used. Here, we highlighted the future perspective and scope for NC@MOF composite catalysis (Table 1).

1. There are still limitations to the encapsulation of NCs into MOFs due to the disruption of NC's guest particles for the growth of MOF. Besides, it is limited to the type and number of MOFs *e.g.*, ZIF-8, ZIF-67, UiO-66, UiO-66-$NH_2$, MOF-108, MIL-101, *etc.* Controlling the both NC structure and MOF and recognizing the active site is still a challenge, however, scope to modulate. By carefully modifying the pore structures, components, and functional groups of the MOF supports, it is possible to substantially enhance and optimize the catalytic activity and selectivity of the immobilized composite.

2. Surface ligands of NCs often pose challenges to catalysis, yet they can also play a role in facilitating the activation of reactants and enabling the regulation of activity and selectivity. The complex role of ligands presents an intriguing subject for future exploration. The aspect of selectivity control is particularly significant and merits systematic examination, given that achieving elevated selectivity is a key aim in catalytic processes.

Table 1 Summary of synthesis procedures of NCs@MOF composite and catalytic applications

| Method of preparation | Composite | Application | Ref. |
|---|---|---|---|
| Surface anchoring | $Au_1Ag_{39}$/ZIF-8, $Ag_{40}$/ZIF-8, $Au_{12}Ag_{32}$/ZIF-8, $Ag_{46}Au_{24}$/ZIF-8, $Au_4Cu_4$/ZIF-8, $Pd_3Cl$/ZIF-8 | Phenylacetylene carboxylation, nitrophenol reduction, and *para*-substituted benzylamine oxidative coupling | 58 |
| | $Au_{25}$(L-Cys)$_{18}$/UiO-66-$NH_2$, $Au_{25}(PET)_{18}$/UiO-66-$NH_2$ | Photocatalytic hydrogen evolution reaction | 60 |
| | $Au_{25}$/ZIF-8 | Reduction of 4-nitrophenol | 62 |
| | $Au_{25}(GSH)_{18}$/MIL-125 (Ti), $Au_{25}(GSH)_{18}$/MIL-101 (Cr), $Au_{25}(GSH)_{18}$/ZIF-8 | Reduction of 4-nitrophenol | 61 |
| | ZIF-8@$Au_{25}$@ZIF-67, ZIF-8@$Au_{25}$@ZIF-8 | Reduction of 4-nitrophenol and carboxylation of terminal alkyne | 63 |
| Solution impregnation | $Au_{133}(SR)_{52}$@bMOF-102/106 | — | 64 |
| | Au NC@ZIF-8, Au NC@ZIF-90 | CO oxidation | 65 |
| Ship in a bottle | $Au_{11}$:$PPh_3$@ZIF-8, $Au_{13}Ag_{12}$:$PPh_3$@MIL-100 | Oxidation of benzyl alcohol | 66 |
| | Au NC@UiO-68-NHC | Photocatalytic $CO_2$ reduction | 67 |
| | AgNC@MIL-125-$NH_2$ | Water purification, hydrogenation of 4-nitroaniline | 68 |
| | Pd@UiO-66-$NH_2$, Pd@UiO-66-$(NH_2)_2$, Pd@UiO-66-$CH_3$, Pd@UiO-66-$(CH_3)_2$ | — | 69 |
| Bottle around a ship | $Au_{12}Ag_{32}(SR)_{30}$@ZIF-8, $Ag_{44}(SR)_{30}$@ZIF-8, $Ag_{12}Cu_{28}(SR)_{30}$@ZIF-8 | $CO_2$ conversion | 59 |
| | $Au_{25}(Capt)_{18}$@UiO-66-X | Oxidative esterification of furfural | 87 |
| | $Au_{38}I(S\text{-}Adm)_{19}$@UiO-66-X, $Au_{38}S(S\text{-}Adm)_{20}$@UiO-66-X, $Au_{38}IS(S\text{-}Adm)_{19}$@UiO-66-X | Reduction of 4-nitrophenol | 70 |
| | $Ag_{25}$@UiO-66-$NH_2$, $AuAg_{24}$@UiO-66-$NH_2$, $PtAg_{24}$@UiO-66-$NH_2$, $PdAg_{24}$@UiO-66-$NH_2$ | Photocatalytic hydrogen production | 70 |
| | $Pt_n$@ZIF-8 ($n \approx 12$) | Catalytic hydrogenation of 1-hexene | 72 |
| | $Co_8Pt_4$@ZIF-8 | — | 73 |
| | Cu NC@UiO-66-$NH_2$, Cu NC@MOF-801 | Photocatalytic $CO_2$ reduction | 74 |
| | $Au_{25}$@Zn-MOF-74, $Au_{25}$@Ni-MOF-74, $Au_{25}$@Co-MOF-74, $Au_{25}$@Mg-MOF-74 | Catalytic reduction of 2-nitro benzonitrile | 76 |

3. Recent research has uncovered instances where the support may actively engage in specific reactions. Analyzing the interactions between ligand-protected NCs and the support (MOFs) is significantly more difficult than assessing bare clusters on supports. Therefore, overcoming the associated challenges through experimental investigation of interfacial processes with computational support will be crucial for future advancements in this area.

4. The catalytic process occurring on NC catalysts will be examined at the atomic level and in real-time. We anticipate that the integration of NC with MOF give rise to a new class of functional composite and uncover the fundamental atomic origins of structure–activity relationships. Ultimately, this advancement will enable chemists to tailor active sites for targeted reactions.

## Data availability

The data used for this feature article will be available on request for academic use.

## Conflicts of interest

There are no conflicts to declare.

## Acknowledgements

AK thanks Anusandhan National Research Foundation (ANRF), New Delhi for a National Post-Doctoral Fellowship (PDF/2023/002916). GJ thanks the MoE, India for Prime Minister Research Fellowship (PMRF).

## References

1 K. N. Ganesh, D. Zhang, S. J. Miller, K. Rossen, P. J. Chirik, M. C. Kozlowski, J. B. Zimmerman, B. W. Brooks, P. E. Savage, D. T. Allen and A. M. Voutchkova-Kostal, *Environ. Sci. Technol. Lett.*, 2021, **8**, 487–491.
2 J. R. Mihelcic, R. O. Barra, B. W. Brooks, M. L. Diamond, M. J. Eckelman, J. MacDonald Gibson, S. Guidotti, A. Ikeda-Araki, M. Kumar, Y. Maiga, J. McConville, S. L. Miller, V. Pizarro, F. Rosario-Ortiz, S. Wang and J. B. Zimmerman, *Environ. Sci. Technol. Lett.*, 2023, **10**, 961–962.
3 K.-G. Liu, Z. Sharifzadeh, F. Rouhani, M. Ghorbanloo and A. Morsali, *Coord. Chem. Rev.*, 2021, **436**, 213827.
4 X. F. Lu, Y. Fang, D. Luan and X. W. D. Lou, *Nano Lett.*, 2021, **21**, 1555–1565.
5 M. A. Abbas, M. Jeon and J. H. Bang, *J. Phys. Chem. C*, 2022, **126**, 16928–16942.
6 Y. Du, H. Sheng, D. Astruc and M. Zhu, *Chem. Rev.*, 2020, **120**, 526–622.
7 Q. Yan, Z. Yuan, Y. Wu, C. Zhou, Y. Dai, X. Wan, D. Yang, X. Liu, N. Xue, Y. Zhu and Y. Yang, *Precis. Chem.*, 2023, **1**, 468–479.
8 D. Yang, J. Wang, Q. Wang, Z. Yuan, Y. Dai, C. Zhou, X. Wan, Q. Zhang and Y. Yang, *ACS Nano*, 2022, **16**, 15681–15704.
9 R. Jin, C. Zeng, M. Zhou and Y. Chen, *Chem. Rev.*, 2016, **116**, 10346–10413.
10 I. Chakraborty and T. Pradeep, *Chem. Rev.*, 2017, **117**, 8208–8271.
11 A. Baghdasaryan and T. Bürgi, *Nanoscale*, 2021, **13**, 6283–6340.
12 X. Sun, P. Wang, X. Yan, H. Guo, L. Wang, Q. Xu, B. Yan, S. Li, J. He, G. Chen, H. Shen and N. Zheng, *iScience*, 2023, **26**, 107850.
13 X. Cai, Y. Sun, J. Xu and Y. Zhu, *Chem. – Eur. J.*, 2021, **27**, 11539–11547.
14 N. Yan, L. Liao, J. Yuan, Y.-J. Lin, L.-H. Weng, J. Yang and Z. Wu, *Chem. Mater.*, 2016, **28**, 8240–8247.
15 H. Liang, Q. Chen, Q.-L. Mo, Y. Wu and F.-X. Xiao, *J. Mater. Chem. A*, 2023, **11**, 9401–9426.
16 M. H. Naveen, R. Khan and J. H. Bang, *Chem. Mater.*, 2021, **33**, 7595–7612.
17 N. Baig, I. Kammakakam and W. Falath, *Mater. Adv.*, 2021, **2**, 1821–1871.
18 A. Kumar and R. Ananthakrishnan, *ACS Appl. Energy Mater.*, 2022, **5**, 2706–2719.
19 H. Chen, L. Zou, E. Hossain, Y. Li, S. Liu, Y. Pu and X. Mao, *Biomater. Sci.*, 2024, **12**, 4283–4300.
20 P. Viswanathan, G. Sivakumar, A. Gowrisankar, R. Tolani, S. Manivannan, K. Kim and R. Ramaraj, *J. Environ. Chem. Eng.*, 2023, **11**, 111431.
21 J. Yang, Y. Peng, S. Li, J. Mu, Z. Huang, J. Ma, Z. Shi and Q. Jia, *Coord. Chem. Rev.*, 2022, **456**, 214391.
22 M. A. Mahmoud, B. Garlyyev and M. A. El-Sayed, *J. Phys. Chem. C*, 2013, **117**, 21886–21893.
23 S. B. Beil, S. Bonnet, C. Casadevall, R. J. Detz, F. Eisenreich, S. D. Glover, C. Kerzig, L. Næsborg, S. Pullen, G. Storch, N. Wei and C. Zeymer, *JACS Au*, 2024, **4**, 2746–2766.
24 G. Deng, H. Yun, M. S. Bootharaju, F. Sun, K. Lee, X. Liu, S. Yoo, Q. Tang, Y. J. Hwang and T. Hyeon, *J. Am. Chem. Soc.*, 2023, **145**, 27407–27414.
25 T. Kawawaki, T. Okada, D. Hirayama and Y. Negishi, *Green Chem.*, 2024, **26**, 122–163.
26 Y.-P. Xie, Y.-L. Shen, G.-X. Duan, J. Han, L.-P. Zhang and X. Lu, *Mater. Chem. Front.*, 2020, **4**, 2205–2222.
27 Y. Wang and T. Bürgi, *Nanoscale Adv.*, 2021, **3**, 2710–2727.
28 Q. Zhu, X. Huang, Y. Zeng, K. Sun, L. Zhou, Y. Liu, L. Luo, S. Tian and X. Sun, *Nanoscale Adv.*, 2021, **3**, 6330–6341.
29 S. Masuda, K. Sakamoto and T. Tsukuda, *Nanoscale*, 2024, **16**, 4514–4528.
30 A. Ma, J. Wang, Y. Wang, Y. Zuo, Y. Ren, X. Ma and S. Wang, *Polyoxometalate*, 2024, **3**, 9140054.
31 Y. Zhang, J. Zhang, Z. Li, Z. Qin, S. Sharma and G. Li, *Chem. Commun.*, 2023, **6**, 24.
32 X. Liu and D. Astruc, *Coord. Chem. Rev.*, 2018, **359**, 112–126.
33 M. A. Habeeb Muhammed and T. Pradeep, *Small*, 2011, **7**, 204–208.
34 R. Tian, S. Zhang, M. Li, Y. Zhou, B. Lu, D. Yan, M. Wei, D. G. Evans and X. Duan, *Adv. Funct. Mater.*, 2015, **25**, 5006–5015.
35 S. Zhao, R. Jin, H. Abroshan, C. Zeng, H. Zhang, S. D. House, E. Gottlieb, H. J. Kim, J. C. Yang and R. Jin, *J. Am. Chem. Soc.*, 2017, **139**, 1077–1080.
36 H. Huang, Z. He, X. Lin, W. Ruan, Y. Liu and Z. Yang, *Appl. Catal., A*, 2015, **490**, 65–70.
37 Z. Bian, N. Dewangan, Z. Wang, S. Pati, S. Xi, A. Borgna, H. Kus and S. Kawi, *ACS Appl. Nano Mater.*, 2021, **4**, 1112–1125.
38 Z. Hong-Cai, L. R. Jeffrey and Y. M. Omar, *Chem. Rev.*, 2012, **112**, 673–674.
39 B. P. Biswal, A. Bhaskar, R. Banerjee and U. K. Kharul, *Nanoscale*, 2015, **7**, 7291–7298.
40 R. Khajavian, M. Mirzaei and H. Alizadeh, *Dalton Trans.*, 2020, **49**, 13936–13947.
41 D. Narváez-Celada and A. S. Varela, *J. Mater. Chem. A*, 2022, **10**, 5899–5917.
42 C. H. Hendon, A. J. Rieth, M. D. Korzyński and M. Dincă, *ACS Cent. Sci.*, 2017, **3**, 554–563.
43 D. Li, H.-Q. Xu, L. Jiao and H.-L. Jiang, *Energy Chem.*, 2019, **1**, 100005.
44 S. Mandal, S. Natarajan, P. Mani and A. Pankajakshan, *Adv. Funct. Mater.*, 2021, **31**, 2006291.
45 T. Islamoglu, S. Goswami, Z. Li, A. J. Howarth, O. K. Farha and J. T. Hupp, *Acc. Chem. Res.*, 2017, **50**, 805–813.
46 Y. Wen, J. Zhang, Q. Xu, X.-T. Wu and Q.-L. Zhu, *Coord. Chem. Rev.*, 2018, **376**, 248–276.
47 L. Chen and Q. Xu, *Matter*, 2019, **1**, 57–89.
48 M. Mukoyoshi and H. Kitagawa, *Chem. Commun.*, 2022, **58**, 10757–10767.
49 Y.-M. Li, J. Hu and M. Zhu, *Coord. Chem. Rev.*, 2023, **495**, 215364.
50 L. Luo and R. Jin, *iScience*, 2021, **24**, 103206.
51 R. K. Aparna, S. Mukherjee, S. S. Rose and S. Mandal, *Inorg. Chem.*, 2022, **61**, 16441–16447.
52 R. K. Aparna, V. Surendran, D. Roy, B. Pathak, M. M. Shaijumon and S. Mandal, *ACS Appl. Energy Mater.*, 2023, **6**, 4072–4078.
53 S. Muhamed, R. K. Aparna, A. Karmakar, S. Kundu and S. Mandal, *Inorg. Chem.*, 2023, **62**, 7195–7202.
54 R. K. Aparna, A. Karmakar, R. T. Arsha, S. Kundu and S. Mandal, *Chem. Commun.*, 2023, **59**, 10444–10447.
55 J. An, O. K. Farha, J. T. Hupp, E. Pohl, J. I. Yeh and N. L. Rosi, *Nat. Commun.*, 2012, **3**, 604.

 

56 A. Dutta, A. G. Wong-Foy and A. J. Matzger, *Chem. Sci.*, 2014, **5**, 3729–3734.
57 S. Øien, D. Wragg, H. Reinsch, S. Svelle, S. Bordiga, C. Lamberti and K. P. Lillerud, *Cryst. Growth Des.*, 2014, **14**, 5370–5372.
58 Y. Yun, Y. Fang, W. Fu, W. Du, Y. Zhu, H. Sheng, D. Astruc and M. Zhu, *Small*, 2022, **18**, 2107459.
59 L. Sun, Y. Yun, H. Sheng, Y. Du, Y. Ding, P. Wu, P. Li and M. Zhu, *J. Mater. Chem. A*, 2018, **6**, 15371–15376.
60 A. Yao, Y. Du, M. Han, Y. Wang, J. Hu, Q. Zhu, H. Sheng and M. Zhu, *Nano Res.*, 2023, **16**, 1527–1532.
61 K. Chu, Y. Luo, D. Wu, Z. Su, J. Shi, J. Z. Zhang and C.-Y. Su, *J. Phys. Chem. Lett.*, 2021, **12**, 8003–8008.
62 Y. Luo, S. Fan, W. Yu, Z. Wu, D. A. Cullen, C. Liang, J. Shi and C. Su, *Adv. Mater.*, 2018, **30**, 1704576.
63 Y. Yun, H. Sheng, K. Bao, L. Xu, Y. Zhang, D. Astruc and M. Zhu, *J. Am. Chem. Soc.*, 2020, **142**, 4126–4130.
64 C. Liu, C. Zeng, T.-Y. Luo, A. D. Merg, R. Jin and N. L. Rosi, *J. Am. Chem. Soc.*, 2016, **138**, 12045–12048.
65 L. Dou, S. Wu, D.-L. Chen, S. He, F.-F. Wang and W. Zhu, *J. Phys. Chem. C*, 2018, **122**, 8901–8909.
66 L. Liu, Y. Song, H. Chong, S. Yang, J. Xiang, S. Jin, X. Kang, J. Zhang, H. Yu and M. Zhu, *Nanoscale*, 2016, **8**, 1407–1412.
67 Y. Jiang, Y. Yu, X. Zhang, M. Weinert, X. Song, J. Ai, L. Han and H. Fei, *Angew. Chem., Int. Ed.*, 2021, **60**, 17388–17393.
68 A. Arenas-Vivo, S. Rojas, I. Ocaña, A. Torres, M. Liras, F. Salles, D. Arenas-Esteban, S. Bals, D. Ávila and P. Horcajada, *J. Mater. Chem. A*, 2021, **9**, 15704–15713.
69 J. King, Z. Lin, F. Zanca, H. Luo, L. Zhang, P. Cullen, M. Danaie, M. Hirscher, S. Meloni, A. M. Elena and P. Á. Szilágyi, *Phys. Chem. Chem. Phys.*, 2024, **26**, 25021–25028.
70 Q. You, H. Wang, Y. Zhao, W. Fan, W. Gu, H.-L. Jiang and Z. Wu, *J. Am. Chem. Soc.*, 2024, **146**, 9026–9035.
71 H. Wang, X. Zhang, W. Zhang, M. Zhou and H.-L. Jiang, *Angew. Chem., Int. Ed.*, 2024, **63**, e202401443.
72 K. Kratzl, T. Kratky, S. Günther, O. Tomanec, R. Zbořil, J. Michalička, J. M. Macak, M. Cokoja and R. A. Fischer, *J. Am. Chem. Soc.*, 2019, **141**, 13962–13969.
73 K. L. Kollmannsberger, Poonam, C. Cesari, R. Khare, T. Kratky, M. Boniface, O. Tomanec, J. Michalička, E. Mosconi, A. Gagliardi, S. Günther, W. Kaiser, T. Lunkenbein, S. Zacchini, J. Warnan and R. A. Fischer, *Chem. Mater.*, 2023, **35**, 5475–5486.
74 S. Dai, T. Kajiwara, M. Ikeda, I. Romero-Muñiz, G. Patriarche, A. E. Platero-Prats, A. Vimont, M. Daturi, A. Tissot, Q. Xu and C. Serre, *Angew. Chem., Int. Ed.*, 2022, **61**, e202211848.
75 H. Zhao, S. Becharef, E. Dumas, F. Carn, G. Patriarche, S. Mura, F. Gazeau, C. Serre and N. Steunou, *Nanoscale*, 2024, **16**, 12037–12049.
76 H. Wang, X. Liu, Y. Zhao, Z. Sun, Y. Lin, T. Yao and H.-L. Jiang, *Natl. Sci. Rev.*, 2024, **11**, nwae252.
77 R.-W. Huang, Y.-S. Wei, X.-Y. Dong, X.-H. Wu, C.-X. Du, S.-Q. Zang and T. C. W. Mak, *Nat. Chem.*, 2017, **9**, 689–697.
78 Z. Chang, X. Jing, C. He, X. Liu and C. Duan, *ACS Catal.*, 2018, **8**, 1384–1391.
79 X.-H. Wu, P. Luo, Z. Wei, Y.-Y. Li, R.-W. Huang, X.-Y. Dong, K. Li, S.-Q. Zang and B. Z. Tang, *Adv. Sci.*, 2019, **6**, 1801304.
80 X.-Y. Dong, H.-L. Huang, J.-Y. Wang, H.-Y. Li and S.-Q. Zang, *Chem. Mater.*, 2018, **30**, 2160–2167.
81 C. Wang, Y.-J. Wang, C.-L. He, Q.-Y. Wang and S.-Q. Zang, *JACS Au*, 2021, **1**, 2202–2207.
82 Z.-Y. Wang, M.-Q. Wang, Y.-L. Li, P. Luo, T.-T. Jia, R.-W. Huang, S.-Q. Zang and T. C. W. Mak, *J. Am. Chem. Soc.*, 2018, **140**, 1069–1076.
83 M. J. Alhilaly, R.-W. Huang, R. Naphade, B. Alamer, M. N. Hedhili, A.-H. Emwas, P. Maity, J. Yin, A. Shkurenko, O. F. Mohammed, M. Eddaoudi and O. M. Bakr, *J. Am. Chem. Soc.*, 2019, **141**, 9585–9592.
84 G. Deng, B. K. Teo and N. Zheng, *J. Am. Chem. Soc.*, 2021, **143**, 10214–10220.
85 X.-H. Ma, J.-Y. Wang, J.-J. Guo, Z.-Y. Wang and S.-Q. Zang, *Chin. J. Chem.*, 2019, **37**, 1120–1124.
86 M. Zhao, S. Huang, Q. Fu, W. Li, R. Guo, Q. Yao, F. Wang, P. Cui, C.-H. Tung and D. Sun, *Angew. Chem., Int. Ed.*, 2020, **59**, 20031–20036.
87 H. Wang, X. Liu, W. Yang, G. Mao, Z. Meng, Z. Wu and H.-L. Jiang, *J. Am. Chem. Soc.*, 2022, **144**, 22008–22017.
88 Y. Zhao, S. Zhuang, L. Liao, C. Wang, N. Xia, Z. Gan, W. Gu, J. Li, H. Deng and Z. Wu, *J. Am. Chem. Soc.*, 2020, **142**, 973–977.
89 W. Zhang, G. Lu, C. Cui, Y. Liu, S. Li, W. Yan, C. Xing, Y. R. Chi, Y. Yang and F. Huo, *Adv. Mater.*, 2014, **26**, 4056–4060.
90 A. Kirchon, L. Feng, H. F. Drake, E. A. Joseph and H.-C. Zhou, *Chem. Soc. Rev.*, 2018, **47**, 8611–8638.
91 Y. Lu, Y. Jiang, X. Gao and W. Chen, *Chem. Commun.*, 2014, **50**, 8464–8467.
92 P. M. Schneider, K. L. Kollmannsberger, C. Cesari, R. Khare, M. Boniface, B. Roldán Cuenya, T. Lunkenbein, M. Elsner, S. Zacchini, A. S. Bandarenka, J. Warnan and R. A. Fischer, *ChemElectroChem*, 2024, **11**, e202300476.
93 Q. Yang, Q. Xu and H.-L. Jiang, *Chem. Soc. Rev.*, 2017, **46**, 4774–4808.
94 S. Yuan, L. Feng, K. Wang, J. Pang, M. Bosch, C. Lollar, Y. Sun, J. Qin, X. Yang, P. Zhang, Q. Wang, L. Zou, Y. Zhang, L. Zhang, Y. Fang, J. Li and H.-C. Zhou, *Adv. Mater.*, 2018, **30**, 1704303.
95 B. Li, J.-G. Ma and P. Cheng, *Small*, 2019, **15**, 1804849.
96 J. Yu, C. Mu, B. Yan, X. Qin, C. Shen, H. Xue and H. Pang, *Mater. Horiz.*, 2017, **4**, 557–569.
97 J. Zhang, X. Cui, Y. Zhou, T. Kong, Y. Wang, X. Wei and Y. Xiong, *Chem. Commun.*, 2023, **59**, 2299–2302.
98 X. Li, Z. Guo, C. Xiao, T. W. Goh, D. Tesfagaber and W. Huang, *ACS Catal.*, 2014, **4**, 3490–3497.